

From Group Sparse Coding to Rank Minimization: A Novel Denoising Model for Low-level Image Restoration

Yunyi Li¹, Guan Gui^{2,*} and Xiefeng Cheng¹

¹ College of Electronic and Optical Engineering & College of Microelectronics, Nanjing University of Posts and Telecommunications, Nanjing 210023, China;

² College of Telecommunications & Information Engineering, Nanjing University of Posts and Telecommunications, Nanjing 210023, China;

*Corresponding Author: guiguan@njupt.edu.cn

Abstract: Recently, low-rank matrix recovery theory has been emerging as a significant progress for various image processing problems. Meanwhile, the group sparse coding (GSC) theory has led to great successes in image restoration (IR) problem with each group contains low-rank property. In this paper, we propose a novel low-rank minimization based denoising model for IR tasks under the perspective of GSC, an important connection between our denoising model and rank minimization problem has been put forward. To overcome the bias problem caused by convex nuclear norm minimization (NNM) for rank approximation, a more generalized and flexible rank relaxation function is employed, namely weighted nonconvex relaxation. Accordingly, an efficient iteratively-reweighted algorithm is proposed to handle the resulting minimization problem combining with the popular $L_{1/2}$ and $L_{2/3}$ thresholding operators. Finally, our proposed denoising model is applied to IR problems via an alternating direction method of multipliers (ADMM) strategy. Typical IR experiments on image compressive sensing (CS), inpainting, deblurring and impulsive noise removal demonstrate that our proposed method can achieve significantly higher PSNR/FSIM values than many relevant state-of-the-art methods.

Keywords: low-rank; group sparse coding; denoising model; weighted nonconvex relaxation; iteratively-reweighted algorithm; ADMM; image restoration.

I. Introduction

Image restoration (IR) problem [1][2][3] is a key topic in low-level visions. The goal of IR is to reconstruct a high-quality image or sequence \mathbf{X} from its various degraded observations \mathbf{Y} . Typical low level IR research includes image compressive sensing (CS) reconstruction [4][5], denoising [6], inpainting [7], deblurring [8] and impulsive noise removal [9], etc. To tackle this typical ill-posed problem, the most popular method is the regularization technique

$$\min_{\mathbf{X}} \{\mathcal{L}(\mathbf{X}) = \mathcal{F}(\mathbf{X}, \mathbf{Y}) + \lambda \mathfrak{R}(\mathbf{X})\} \quad (1)$$

where $\mathcal{F}(\mathbf{X}, \mathbf{Y})$ denotes the fidelity term which can penalize our desired image or sequence \mathbf{X} far from the original degraded \mathbf{Y} , the second term $\mathfrak{R}(\mathbf{X})$ is the regularization term which can provide the necessary prior knowledge of image, e.g., the sparsity, smoothness or continuity, and the regularization parameter λ can make the tradeoff between the first fidelity term and the second regularization term.

It is well documented that how to exploit more prior knowledge for the minimization of

problem (1) is at the core, in the past several years, how to design the regularization term to exploit the prior of an image in a predefined domain has been widely studied. Sparsity-inducing approach has been widely exploited in various sparse signal recovery and IR applications [10][11][12][13], e.g. the L_1 -norm based regularization, the nonconvex penalized regularization of L_p -norm [14], Smoothly Clipped Absolute Deviation (SCAD) [15], Logarithm [16], and Minimax Concave Penalty (MCP) [17], utilize the sparsity as prior for minimization. However, these traditional regularization term for IR approaches can only exploit a few structural features of image and some important artifacts will not be preserved. Besides the sparsity based prior model, another popular prior models to exploit the nonlocal self-similarity features of image patches, which can provide more prior knowledge to improve the restoration quality and the promising performance has been well documented [18]. Very recently, the sparsity and the nonlocal self-similarity features often exploit simultaneously to product better approximation [19], one of the state-of-the-art models is the non-locally centralized sparse representation (NCSR) model proposed in [20], which can exploit the nonlocal self-similarity of image to earn a more accurate sparse representation coefficient, and then centralize the sparse coefficients of the degraded image to the restored image, and has shown its promising performance. In [21], a novel and efficient framework is proposed for IR based on group sparse coding (GSC) model, where the image can be sparsely represented as a linear combination in the domain of group.

Although the well-known GSC based model has shown the significant improvements for IR tasks, the important low-rank property of each group is not being used, and still minimizing the optimization problem from the perspective of sparsity. According to the concept of image group matrix, for any given image, the adjacent patches have similar structures, and similar patches can be grouped into a matrix after vectorizing processing, such that the matrix shows low-rank property, then matrix competition for each group can be conducted to recover the desired image. The last decades has seen the group based low-rank minimization method for image and video restoration with the development of the theory of compressive sensing and GSC [22][23][24][25]. Like the L_0 -norm regularized minimization problem, it is not tractable to minimize the rank regularized problem because of the property of nonconvex and discontinuous of $rank(\mathbf{X})$, and is usually relaxed to the convex nuclear norm minimization (NNM) model. However, the most popular convex NNM often leads to a biased solution, since NNM is usually over-shrink the singular values and treats each of them equally, while larger singular values actually quantify the main preserved information. To tackle this problem, various low-rank relaxations have been proposed, the weighted nuclear norm (WNN) [6], the truncated nuclear norm (TNN) [26], the Schatten- p nuclear norm (Sp -NN) [27], and the generalized nonconvex nonsmooth functions on singular values (e.g., L_p , SCAD, MCP and Logarithm, e.t.,) [28][29][11].

Recently works tend to exploit the theoretic connection and relationship among various sparsity models and low-rank models. Zha et al. [30][31] answer this important question and build a theoretical benchmark for sparse coding and low-rank minimization from the perspective of GSC. Wen et al. [32] build a more general theoretic relationship between various prior models of sparsity and low-rank model. In this paper, motivated by the simplest and typical denoising model in IR problem, we try to bridge the gap between sparsity prior model and low-rank minimization schemes from a new perspective of denoising model via the famous GSC theory, which will convert the traditional sparse coding denoising problem into the low-rank regularization model. Then a framework is designed for IR applications by combining the alternating direction method of

multipliers (ADMM). Our IR framework not only can unify the local sparsity and nonlocal similarity of image simultaneously as image prior, but also can reconstruct image using various matrix competition approaches for rank approximation. Our contributions in this paper can be summarized as:

(1) We propose a novel denoising model base on the GSC framework via rank minimization. In which, we convert the sparsity-inducing optimization problem into the low-rank matrix minimization problem via an effective dictionary learning approach. We also give a theoretical analysis about their connection and relationship between the denoising model and low-rank minimization scheme.

(2) To achieve an accurate approximation of the rank of group matrix for our denoising model, we propose a generalized low-rank minimization model. Our proposed model employs a generalized and flexible weighted scheme and a generalized nonconvex nonsmooth surrogate function on singular values of the group matrix. To solve the generalized rank minimization problem for GSC, we will first convert the optimization model into a GSC based derivative double nonconvex nonsmooth rank (GSC-DNNR) minimization problem, and then develop an iterative reweighted singular-value function thresholding algorithm.

(3) We address the IR problem using our proposed denoising model, an alternative direction method of multipliers (ADMM) framework is integrated, where the sparse coding for GSC based denoising model and the group matrix of desired image will be achieved simultaneously. We further evaluate the proposed framework for four classic IR problems, including image CS reconstruction, inpainting, deblurring, and impulsive noise removal.

The flowchart of our proposed methods for IR problem by rank minimization based GSC denoising model is presented in the Fig. 1.

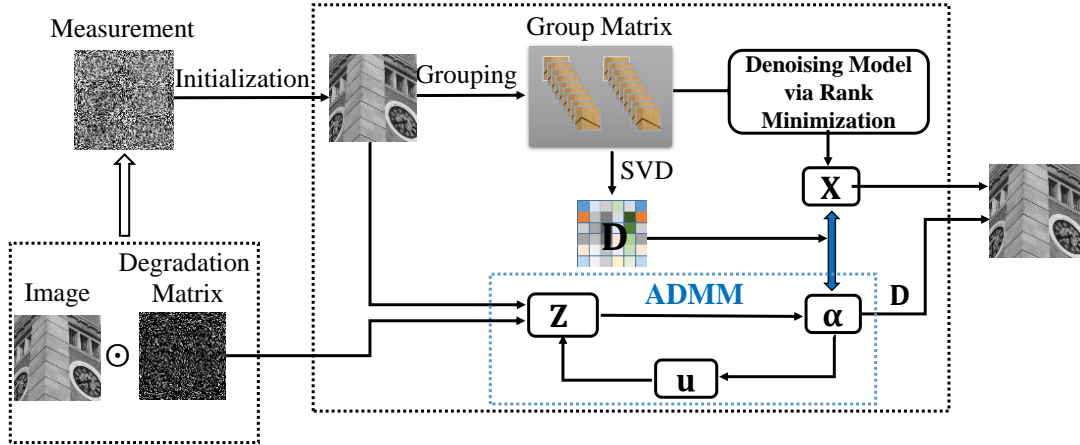


Fig. 1. Flowchart of our proposed model for IR problem.

The rest of our paper is as follows. In the section II, we will first introduce the GSC theory, and then propose a GSC based denoising model, and give a theoretical derivation about connection between our proposed denoising model and low-rank minimization problem. Then we exploit a weighted nonconvex relaxation for rank approximation of group matrix and develop an iteratively-reweighted singular-value thresholding algorithm for the GSC based nonconvex nonsmooth low-rank minimization problem. In the section III, we will introduce how to employ our proposed

denoising model for IR problems via ADMM framework. In the section IV, we will evaluate the effectiveness of our proposed method for various IR tasks and compare the performance with current state-of-the-art IR algorithms. Finally, a brief summary will be made in section V.

II. Group Sparse Coding based Denoising Model via Rank

Minimization

This section will introduce the basic theory of group sparse coding, and then a self-adaptive dictionary learning strategy is introduced for each group. The GSC problem can be converted into the low-rank matrix recovery problem via our proposed adaptive dictionary learning scheme.

2.1. Group sparse coding

Concretely, we first divide the original image $\mathbf{X} \in \mathbb{R}^{\sqrt{N} \times \sqrt{N}}$ into n overlapping patches $\mathbf{X}_k, k = 1, 2, \dots, n$, with the size is $\sqrt{B_s} \times \sqrt{B_s}, B_s < N$. For each patch \mathbf{X}_k , there exist c best matched patches, we denote the set of these patches as $S_{\mathbf{x}_k}$, then we search them in a given searching window with the size of $L \times L$ using the well-known Euclidean distance as the similarity criterion. Next, these similar patches will be stacked into a group matrix with the size of $B_s \times c$, denoted by $\mathbf{X}_{G_k} = [\mathbf{X}_{G_k,1}, \mathbf{X}_{G_k,2}, \dots, \mathbf{X}_{G_k,c}] \in \mathbb{R}^{B_s \times c}$, where each patch will be vectorized as $\mathbf{X}_{G_k,i} \in \mathbb{R}^{B_s \times 1}, i = 1, 2, \dots, c$ as the columns. Then the constructed group matrix \mathbf{X}_{G_k} consisting of c patches containing similar structures, the construction process of group can be expressed as

$$\mathbf{X}_{G_k} = G_k(\mathbf{X}), k = 1, 2, \dots, n. \quad (2)$$

where the operator $G_k(\cdot)$ denotes the group construction from \mathbf{X} . **Fig. 2** illustrates the construction process of group.

Conversely, if we average all the group \mathbf{X}_{G_k} , we can achieve the original image \mathbf{X} by

$$\mathbf{X} = \sum_{k=1}^n \mathcal{R}_k^T(\mathbf{X}_{G_k}) ./ \sum_{k=1}^n \mathcal{R}_k^T(\mathbf{1}_{B_s}) \quad (3)$$

where $\mathcal{R}_k^T(\cdot)$ denotes the transpose grouping operator, $\mathbf{1}_{B_s} \in \mathbb{R}^{B_s \times c}$ stands for a matrix with all the elements are 1, and operator $./$ denotes an element-wise division of two matrix.

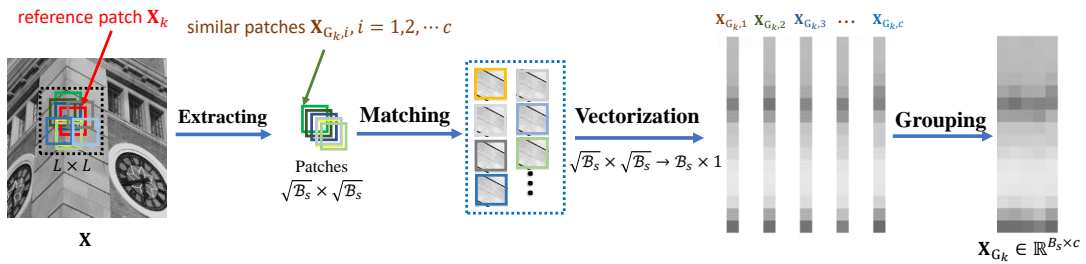


Fig. 2. Illustrations of generating group matrix.

According to sparse coding theory, it is expected that the coefficient vector is as sparse as possible with the group \mathbf{X}_{G_k} can be faithfully represented by the dictionary \mathbf{D}_{G_k} . To obtain an adaptive dictionary \mathbf{D}_{G_k} for each group \mathbf{X}_{G_k} , in this paper, we adopt a self-adaptive dictionary learning scheme [33] for each group, and learn the adaptive dictionary \mathbf{D}_{G_k} from \mathbf{X}_{G_k} directly. We first conduct the singular value decomposition (SVD) of \mathbf{X}_{G_k} by

$$\mathbf{X}_{G_k} = \mathbf{U}_{\mathbf{X}_{G_k}} \mathbf{\Sigma}_{\mathbf{X}_{G_k}} \mathbf{V}_{\mathbf{X}_{G_k}}^T = \sum_{i=1}^m \sigma_{\mathbf{X}_{G_k},i} \mathbf{u}_{\mathbf{X}_{G_k},i} \mathbf{v}_{\mathbf{X}_{G_k},i}^T \quad (4)$$

where $m = \min(B_s, c)$, $\mathbf{U}_{G_k} = [\mathbf{u}_{X_{G_k,1}}, \mathbf{u}_{X_{G_k,2}}, \dots, \mathbf{u}_{X_{G_k,m}}]$, $\mathbf{V}_{X_{G_k}} = [\mathbf{v}_{X_{G_k,1}}, \mathbf{v}_{X_{G_k,2}}, \dots, \mathbf{v}_{X_{G_k,m}}]$ and $\boldsymbol{\Sigma}_{X_{G_k}} = \text{diag}([\sigma_{X_{G_k,1}}, \sigma_{X_{G_k,2}}, \dots, \sigma_{X_{G_k,m}}])$. Then, the atom \mathbf{d}_{G_k} of the dictionary \mathbf{D}_{G_k} can be obtained by

$$\mathbf{d}_{G_k,i} = \mathbf{u}_{X_{G_k,i}} \mathbf{v}_{X_{G_k,i}}^T, \quad i = 1, 2, \dots, m \quad (5)$$

Finally, we can achieve the self-adaptive dictionary for each group by

$$\mathbf{D}_{G_k} = [\mathbf{d}_{G_k,1}, \mathbf{d}_{G_k,2}, \dots, \mathbf{d}_{G_k,m}]. \quad (6)$$

It should be noted that every atom $\mathbf{d}_{G_k,i} \in \mathbb{R}^{B_s \times c}$, $i = 1, 2, \dots, m$ in the dictionary \mathbf{D}_{G_k} is a matrix with the same size of group \mathbf{X}_{G_k} . After obtaining the dictionary $\mathbf{D}_{G_k} = [\mathbf{d}_{G_k,1}, \mathbf{d}_{G_k,2}, \dots, \mathbf{d}_{G_k,m}] \in \mathbb{R}^{(B_s \times c) \times m}$, the representation coefficient vector can be achieved by

$$\hat{\boldsymbol{\alpha}}_{G_k} = \arg \min_{\boldsymbol{\alpha}_{G_k}} \frac{1}{2} \|\mathbf{X}_{G_k} - \mathbf{D}_{G_k} \boldsymbol{\alpha}_{G_k}\|_2^2 + \lambda \|\boldsymbol{\alpha}_{G_k}\|_0, \quad k = 1, 2, \dots, n. \quad (7)$$

in which $\boldsymbol{\alpha}_{G_k} \in \mathbb{R}^{m \times 1}$ is the achieved sparse coefficient vector. Then the image group will be represented sparsely by

$$\mathbf{X}_{G_k} = \mathbf{D}_{G_k} \hat{\boldsymbol{\alpha}}_{G_k} = \sum_{i=1}^m \alpha_{G_k,i} \mathbf{d}_{G_k,i} \quad (8)$$

where $\mathbf{D}_{G_k} = [\mathbf{d}_{G_k,1}, \dots, \mathbf{d}_{G_k,m}] \in \mathbb{R}^{(B_s \times c) \times m}$ denotes the dictionary, and $\hat{\boldsymbol{\alpha}}_{G_k} = [\hat{\alpha}_{G_k,1}, \hat{\alpha}_{G_k,2}, \dots, \hat{\alpha}_{G_k,m}] \in \mathbb{R}^{m \times 1}$ is the desired vector.

For simplify, if we concatenate all the corresponding dictionary \mathbf{D}_{G_k} as \mathbf{D}_G , and the original entire image \mathbf{X} can be represented by

$$\mathbf{X} = \mathbf{D}_G \circ \boldsymbol{\alpha}_G \quad (9)$$

where $\boldsymbol{\alpha}_G$ denotes the concatenation of all \mathbf{D}_{G_k} . As a result, the learned self-adaptive dictionary will build the link between the GSC problem and rank minimization problem.

2.2. GSC based denoising model via low-rank minimization

In practice, the original image \mathbf{X} and the corresponding groups \mathbf{X}_{G_k} , $k = 1, 2, \dots, n$. are unknown, considering the following GSC based denoising model

$$\hat{\boldsymbol{\alpha}}_{G_k} = \arg \min_{\boldsymbol{\alpha}_{G_k}} \frac{1}{2} \|\mathbf{Y}_{G_k} - \mathbf{D}_{G_k} \boldsymbol{\alpha}_{G_k}\|_2^2 + \lambda \|\boldsymbol{\alpha}_{G_k}\|_0, \quad k = 1, 2, \dots, n. \quad (10)$$

where $\mathbf{Y}_{G_k} \in \mathbb{R}^{B_s \times c}$ denotes the degraded observation of \mathbf{X}_{G_k} , $\boldsymbol{\alpha}_{G_k}$ denotes the sparse coefficient vector over the dictionary \mathbf{D}_{G_k} , and λ denotes the regularization parameter. Through the GSC model, we can estimate the latent image \mathbf{X}_{G_k} over the adaptive dictionary \mathbf{D}_{G_k} from its degraded observation \mathbf{Y}_{G_k} , then the desired matrix (group) can be reconstructed by $\hat{\mathbf{X}}_{G_k} = \mathbf{D}_{G_k} \hat{\boldsymbol{\alpha}}_{G_k}$.

Remark 2.1. For any image group matrix \mathbf{X}_{G_k} and its singular value decomposition (SVD)

$\mathbf{X}_{G_k} = \sum_{i=1}^m \sigma_{X_{G_k,i}} \mathbf{u}_{X_{G_k,i}} \mathbf{v}_{X_{G_k,i}}^T$, if $\mathbf{X}_{G_k} = \mathbf{D}_{G_k} \boldsymbol{\alpha}_{G_k}$, then the number of nonzero elements of $\boldsymbol{\alpha}_{G_k}$ is

equal to the number of nonzero value of singular values $\sigma_{X_{G_k,i}}$, we have the following relationship

$$\|\boldsymbol{\alpha}_{G_k}\|_0 = \text{rank} \left(\sum_{i=1}^m \sigma_{X_{G_k,i}} \mathbf{d}_{G_k,i} \right) = \text{rank}(\mathbf{D}_{G_k} \boldsymbol{\alpha}_{G_k}) = \text{rank}(\mathbf{X}_{G_k}) \quad (11)$$

where $\boldsymbol{\alpha}_{G_k} = [\alpha_{G_k,1}, \alpha_{G_k,2}, \dots, \alpha_{G_k,m}] \in \mathbb{R}^{m \times 1}$, $\mathbf{D}_{G_k} = [\mathbf{d}_{G_k,1}, \dots, \mathbf{d}_{G_k,m}] \in \mathbb{R}^{(B_s \times c) \times m}$, and $\text{rank}(\mathbf{X}_{G_k})$ denotes the singular value number of the matrix \mathbf{X}_{G_k} .

Benefiting from the fact that the degraded group \mathbf{Y}_{G_k} and original group \mathbf{X}_{G_k} share the same coding dictionary \mathbf{D}_{G_k} , according to the relationship in the **Remark 2.1**, by substituting $\mathbf{D}_{G_k}\boldsymbol{\alpha}_{G_k}$ using \mathbf{X}_{G_k} in (10), the denoising problem (10) can be converted into the following equivalent low-rank minimization

$$\hat{\mathbf{X}}_{G_k} = \arg \min_{\mathbf{X}_{G_k}} \frac{1}{2} \|\mathbf{Y}_{G_k} - \mathbf{X}_{G_k}\|_F^2 + \lambda \text{rank}(\mathbf{X}_{G_k}), k = 1, 2, \dots, n. \quad (12)$$

where \mathbf{X}_{G_k} denotes the constructed image group with low-rank property, and \mathbf{Y}_{G_k} denotes the corresponding observation group. It is worth noting that the sparse coefficient vector $\boldsymbol{\alpha}_{G_k}$ is also the singular value vector of matrix \mathbf{X}_{G_k} in our proposed model. Then we can convert the sparsity-inducing optimization problem (10) into the low-rank minimization problem (12).

The low-rank minimization problem (12) is a NP-hard problem, which is usually relaxed as a convex NNM problem,

$$\hat{\mathbf{X}}_{G_k} = \arg \min_{\mathbf{X}_{G_k}} \frac{1}{2} \|\mathbf{Y}_{G_k} - \mathbf{X}_{G_k}\|_F^2 + \lambda \|\mathbf{X}_{G_k}\|_* \quad (13)$$

where, $\|\mathbf{X}_{G_k}\|_* = \sum_{i=1}^{\min(B_s, c)} |\sigma_i(\mathbf{X}_{G_k})|$ denotes the nuclear norm, and $\sigma_i(\mathbf{X}_{G_k}), i = 1, 2, \dots$, are the singular values of \mathbf{X}_{G_k} , and $\|\cdot\|_F$ presents the Frobenius norm. Many recent works tend to use the improved NNM for low-rank minimization, e.g., the truncated nuclear norm (TNN) [26], the Schatten p -norm (S_p) [27], the weighted nuclear norm (WNN) [6], and so on. It is well documented that the WNN based method can often earn the best performance among them [6]. What's more, some popular nonconvex counterparts of L_0 -norm on singular value have shown great potentials to improve the rank minimization performance [28][29], typical nonconvex surrogate functions include L_p -norm [14], SCAD [15], Logarithm [16], MCP [17]. Motivated by the weighted strategy and the nonconvex counterparts of L_0 -norm, this paper uses a more generalized and flexible rank relaxation function for rank approximation of the group matrix using weighted nonconvex relaxation, such that

$$\hat{\mathbf{X}}_{G_k} = \arg \min_{\mathbf{X}_{G_k}} \frac{1}{2} \|\mathbf{Y}_{G_k} - \mathbf{X}_{G_k}\|_F^2 + \lambda \boldsymbol{\rho}_{\mathbf{w}_k}(\sigma(\mathbf{X}_{G_k})) \quad (14)$$

in which, $\boldsymbol{\rho}_{\mathbf{w}_k}(\sigma(\mathbf{X}_{G_k})) = \sum_{i=1}^r w_{k,i} \rho(\sigma_{k,i})$, $r = \min(B_s, c)$, $\mathbf{w}_k = (w_{k,1}, w_{k,2}, \dots, w_{k,r})$ is the weighting vector with $w_{k,1} \leq w_{k,2} \leq \dots \leq w_{k,r}$, $\sigma(\mathbf{X}_{G_k}) = (\sigma_{k,1}, \sigma_{k,2}, \dots, \sigma_{k,r})$ denotes the singular value vector with $\sigma_{k,1} \leq \sigma_{k,2} \leq \dots \leq \sigma_{k,r}$, the function $\rho(\cdot): \mathbb{R}^+ \rightarrow \mathbb{R}^+$ is the proper and lower semi-continuous function, and is nondecreasing on $[0, +\infty)$. It should be noted that the nonconvexity of the function $\rho(\cdot)$ is often weaker than traditional nonconvex functions, e.g., L_p -norm, MCP and SCAD. According to the definition of the rank relaxation function, $\boldsymbol{\rho}_{\mathbf{w}}(\cdot)$ will be more flexible with different w_i and $\rho(\cdot)$. When $\rho(\cdot)$ is the absolute function, $\boldsymbol{\rho}_{\mathbf{w}}(\cdot)$ becomes the traditional nuclear norm and the weighted nuclear norm with all $w_i = 1$ and not all $w_{k,i} = 1$, respectively. When $\rho(\cdot)$ is the L_p -norm with $0 < p < 1$, $\boldsymbol{\rho}_{\mathbf{w}}(\cdot)$ will become the Schatten p -nuclear norm and the weighted Schatten p -nuclear norm with all $w_{k,i} = 1$ and not all $w_{k,i} = 1$, respectively. Moreover, when the weighting vector \mathbf{w} with partial $w_{k,i} = 0$, $\boldsymbol{\rho}_{\mathbf{w}}(\cdot)$ will become the truncated nuclear norm and the truncated Schatten p -nuclear norm with $p = 1$ and $0 < p < 1$, respectively. A summarization for these special cases can be found in the **Table 1**. Our proposed model can estimate the rank of each group with a high accurate and nearly unbiased solution, one popular example is the weighting vector \mathbf{w}_k is inversely proportional to the corresponding singular

values, e.g., $\omega_{k,i} = \mathbf{1}/(|\sigma_i(\mathbf{X}_{G_k})| + \varepsilon)$ [6].

Table 1. Different relaxation functions with different weight w and relaxation function ρ .

Name	Relaxation Function	w	ρ	$\partial\rho$
Nuclear norm	$\ \mathbf{X}\ _* = \sum_{i=1}^m \sigma_i(\mathbf{X})$	$w_i = 1, i = 1, 2, \dots, m$	$\rho(\sigma_i) = \sigma_i,$ $(i = 1, \dots, m)$	$\partial\rho(\sigma_i) = \sigma_i,$ $(i = 1, \dots, m)$
Weighted nuclear norm	$\ \mathbf{X}\ _{w,*} = \sum_{i=1}^m w_i \sigma_i(\mathbf{X})$	$w_i \geq 0, i = 1, 2, \dots, m$	$\rho(\sigma_i) = \sigma_i,$ $(i = 1, \dots, m)$	$\partial\rho(\sigma_i) = \sigma_i,$ $(i = 1, \dots, m)$
Truncated nuclear norm	$\ \mathbf{X}\ _r = \sum_{i=r+1}^m \sigma_i(\mathbf{X})$	$w_i = 1, i = r+1, \dots, m$	$\rho(\sigma_i) = \begin{cases} 0, & i = 1, \dots, r \\ \sigma_i, & i = r+1, \dots, m \end{cases}$	$\partial\rho(\sigma_i) = \begin{cases} 0, & i = 1, \dots, r \\ 1, & i = r+1, \dots, m \end{cases}$
Weighted Truncated nuclear norm	$\ \mathbf{X}\ _{w,r} = \sum_{i=r+1}^m w_i \sigma_i(\mathbf{X})$	$w_i \geq 0, i = r+1, \dots, m$	$\rho(\sigma_i) = \begin{cases} 0, & i = 1, \dots, r \\ \sigma_i, & i = r+1, \dots, m \end{cases}$	$\partial\rho(\sigma_i) = \begin{cases} 0, & i = 1, \dots, r \\ 1, & i = r+1, \dots, m \end{cases}$
Schatten p -norm	$\ \mathbf{X}\ _p^p = \sum_{i=1}^m (\sigma_i(\mathbf{X}))^p$	$w_i = 1, i = 1, 2, \dots, m$	$\rho(\sigma_i) = (\sigma_i)^p,$ $(i = 1, \dots, m)$	$\partial\rho(\sigma_i) = p(\sigma_i)^{p-1},$ $(i = 1, \dots, m)$
Weighted Schatten p -norm	$\ \mathbf{X}\ _{w,sp}^p = \sum_{i=1}^m w_i (\sigma_i(\mathbf{X}))^p$	$w_i \geq 0, i = 1, 2, \dots, m$	$\rho(\sigma_i) = (\sigma_i)^p,$ $(i = 1, \dots, m)$	$\partial\rho(\sigma_i) = p(\sigma_i)^{p-1},$ $(i = 1, \dots, m)$

Actually, according to the reweighted strategy [28] and the super-gradient properties [28], the problem (14) can be intrinsically derived from the following nonconvex nonsmooth rank minimization problem [34][35], e.g.,

$$\hat{\mathbf{X}}_{G_k} = \arg \min_{\mathbf{X}_{G_k}} \frac{1}{2} \|\mathbf{Y}_{G_k} - \mathbf{X}_{G_k}\|_F^2 + \lambda \sum_{i=1}^r h(\rho(\sigma_i(\mathbf{X}_{G_k}))) \quad (15)$$

where $h(\rho(\cdot))$ denotes the relaxation function, and in this paper, we choose $h(\cdot) = \rho(\cdot)$ without loss of the generality, in which, $\rho(\cdot)$ denotes a function with lower semi-continuous property in $[0, +\infty)$. As a result, the problem (15) can be substituted by

$$\hat{\mathbf{X}}_{G_k} = \arg \min_{\mathbf{X}_{G_k}} \frac{1}{2} \|\mathbf{Y}_{G_k} - \mathbf{X}_{G_k}\|_F^2 + \lambda \sum_{i=1}^r \rho(\sigma_i(\mathbf{X}_{G_k})). \quad (16)$$

in which, there exist two relaxation function $\rho(\cdot)$, thus (16) can be known as the GSC based double nonconvex nonsmooth rank (GSC-DNNR) minimization problem.

2.3. GSC-DNNR minimization for denoising model

The GSC-DNNR minimization problem (16) is more difficult to resolve than traditional convex NNM problem. To solve this problem, we usually need to convert the minimization problem into the iteratively reweighted minimization problem, which benefits from the antimotone property of relaxation function $\rho(\cdot)$ and the supergradient function $\partial\rho(\cdot)$. We first give the following theorem.

Lemma 2.1. [28] *Let $\rho(\cdot): \mathbb{R}^+ \rightarrow \mathbb{R}^+$ be concave with the monotonical nondecreasing property, and its supergradient $\partial\rho(\cdot)$ is monotonically nonincreasing on $[0, +\infty)$, then we have*

$$\rho(s_1) - \rho(s_2) \leq w_{s_2} (s_1 - s_2) \quad (17)$$

where $w_{s_2} \in \partial\rho(s_2)$, s_1 and s_2 denote two any given values.

Since the monotonical nondecreasing property of $\rho(\cdot)$ and the monotonical nonincreasing property of $\partial\rho(\cdot)$, for any given $\sigma_1 \geq \sigma_2 \geq \dots \geq \sigma_r$, we have $\rho(\sigma_1) \geq \rho(\sigma_2) \geq \dots \geq \rho(\sigma_r)$ and $\partial\rho(\rho(\sigma_1)) \leq \partial\rho(\rho(\sigma_2)) \leq \dots \leq \partial\rho(\rho(\sigma_r))$, that is to say, the function of $\partial\rho(\rho(\cdot))$ is monotonical nonincreasing on $[0, +\infty)$. Then according to the **Lemma 2.1**, if we replace the value s_1 and s_2 by $\rho(s_1)$ and $\rho(s_2)$, and substrate the weighting $w_{s_2} \in \partial\rho(s_2)$ by $w_{\rho(s_2)} \in \partial\rho(\rho(s_2))$. Then we have the following theorem.

Lemma 2.2. [35] *Let $\rho(\cdot): \mathbb{R}^n \rightarrow \mathbb{R}$ be concave with the monotonical nondecreasing property, its supergradient $\partial\rho(\cdot)$ is monotonically nonincreasing on $[0, +\infty)$, and the double supergradient $\partial\rho(\rho(\cdot))$ is monotonically nonincreasing on $[0, +\infty)$, then we have*

$$\rho(\rho(s_1)) - \rho(\rho(s_2)) \leq w_{\rho(s_2)} (\rho(s_1) - \rho(s_2)) \quad (18)$$

where $w_{\rho(s_2)} \in \partial\rho(\rho(s_2))$, s_1 and s_2 denote two any given values.

According to the **Lemma 2.2**, since the relaxation function of $\rho(\cdot)$ is concave on $[0, +\infty)$, then according to the monotonical nondecreasing property of double supergradient $\partial\rho(\rho(\cdot))$. As a result, we have

$$\rho\left(\rho\left(\sigma_i(\mathbf{X}_{G_k})\right)\right) \leq \rho\left(\rho\left(\sigma_i(\mathbf{X}_{G_k}^t)\right)\right) + w_{k,i}^t \left(\rho\left(\sigma_i(\mathbf{X}_{G_k})\right) - \rho\left(\sigma_i(\mathbf{X}_{G_k}^t)\right)\right) \quad (19)$$

where $w_{k,i}^t \in \partial\rho\left(\rho\left(\sigma_i(\mathbf{X}_{G_k}^t)\right)\right)$ with $w_{k,1}^t \leq w_{k,2}^t \leq \dots \leq w_{k,r}^t$. Then the problem (16) can be relaxed as the following optimization problem, e.g.,

$$\begin{aligned} \mathbf{X}_{G_k}^{t+1} &= \arg \min_{\mathbf{X}_{G_k}} \frac{1}{2} \|\mathbf{Y}_{G_k} - \mathbf{X}_{G_k}\|_F^2 + \lambda \sum_{i=1}^r \left\{ \rho\left(\rho\left(\sigma_i(\mathbf{X}_{G_k}^t)\right)\right) + w_{k,i}^t \left(\rho\left(\sigma_i(\mathbf{X}_{G_k})\right) - \rho\left(\sigma_i(\mathbf{X}_{G_k}^t)\right)\right) \right\} \\ &= \arg \min_{\mathbf{X}_{G_k}} \frac{1}{2} \|\mathbf{Y}_{G_k} - \mathbf{X}_{G_k}\|_F^2 + \lambda \sum_{i=1}^r w_{k,i}^t \rho\left(\sigma_i(\mathbf{X}_{G_k})\right) \end{aligned} \quad (20)$$

in which, the iteratively-weighting vector can be updated by $w_{k,i}^{t+1} \in \partial\rho\left(\rho\left(\sigma_i(\mathbf{X}_{G_k}^{t+1})\right)\right)$, and $\mathbf{X}_{G_k}^t$ denotes the k -th iteration of variable \mathbf{X}_{G_k} .

Essentially, to solve (20) is equivalent to solving a proximal operator. Some previous works have been studied to solve the (20) for some special cases of the relaxation functions, such as the iteratively reweighted nuclear norm (IRNN) algorithm (Lu et, al. [28]). Here, we will develop our algorithm for GSC proposed in Zhang et, al [35], which can be a extend version of Lu's IRNN method (Lu et, al. [28]). We will present that, if the singular-value function thresholding operator is monotone, the problem (20) can be resolved by the weighted operator.

Theorem 2.1. [29] *Let a function $\rho(\cdot): \mathbb{R}^n \rightarrow \mathbb{R}$ such that a proximal operator $\text{Prox}_{w_i, \rho}^{\delta_i}(\cdot)$*

is monotone, i.e., $\text{Prox}_{w_1, \rho}^{\delta_1}(\delta_1) > \text{Prox}_{w_2, \rho}^{\delta_2}(\delta_2)$ for any $\delta_1 > \delta_2$. For any given $\lambda > 0$, $\mathbf{Y} \in \mathbb{R}^{m \times n}$, $r = \min(m, n)$, the weighting values with $w_1 \leq w_2 \leq \dots \leq w_r$. Let $\mathbf{Y} = \mathbf{U} \text{Diag}(\boldsymbol{\delta}(\mathbf{Y})) \mathbf{V}^T$ is the SVD of \mathbf{Y} , and the singular values satisfy $\delta_1(\mathbf{Y}) \geq \delta_2(\mathbf{Y}) \geq \dots \geq \delta_r(\mathbf{Y})$, then the solution to

$$\mathbf{X} = \arg \min_{\mathbf{X}} \frac{\lambda}{2} \|\mathbf{X} - \mathbf{Y}\|_F^2 + \lambda \sum_{i=1}^r w_i \rho(\sigma_i(\mathbf{X})) \quad (21)$$

is

$$\mathbf{X}^* = \mathbf{U} \text{Diag}(\boldsymbol{\delta}_i^*) \mathbf{V}^T \quad (22)$$

where $\boldsymbol{\delta}_i^*$ can be obtained by

$$\delta_i^* \in \text{Prox}_{w_i, \rho}^{\delta_i}(\delta_i(\mathbf{Y})) = \arg \min_{\sigma_i > 0} \frac{1}{2} (\sigma_i(\mathbf{X}) - \delta_i(\mathbf{Y}))^2 + \lambda w_i \rho(\sigma_i(\mathbf{X})) \quad (23)$$

It follows from the **Theorem 2.1.**, considering the problem (20), since $w_{k,1}^t \leq w_{k,2}^t \leq \dots \leq w_{k,r}^t$, and $\rho(\cdot): \mathbb{R}^n \rightarrow \mathbb{R}$ and the proximal operator $\text{Prox}_{w_i, \rho}^{\delta_i}(\cdot)$ is monotone. Then the optimal solution of our optimization problem (20) can be eventually achieved by

$$\mathbf{X}_{G_k}^{t+1} = \mathbf{U} \text{Diag} \left(\text{Prox}_{w_{k,i}, \rho}^{\delta_i} \left(\boldsymbol{\delta}(\mathbf{Y}_{G_k}^t) \right) \right) \mathbf{V}^T \quad (24)$$

where $\text{Prox}_{w_{k,i}\rho}^{\delta}(\boldsymbol{\delta}(\mathbf{Y}_{G_k}^t))$ denotes the element-wise operator, e.g.,

$$\text{Prox}_{w_{k,i}\rho}^{\delta_i}(\boldsymbol{\delta}_i(\mathbf{Y}_{G_k}^t)) = \arg \min_{\delta_i > 0} \frac{1}{2} (\sigma_i(\mathbf{X}_{G_k}) - \delta_i(\mathbf{Y}_{G_k}^t))^2 + \lambda w_{k,i}^t \rho(\sigma_i(\mathbf{X}_{G_k})) \quad (25)$$

where $\delta_1(\mathbf{Y}_{G_k}^t) \geq \delta_2(\mathbf{Y}_{G_k}^t) \geq \dots \geq \delta_r(\mathbf{Y}_{G_k}^t)$.

2.4. $L_{1/2}$ and $L_{2/3}$ thresholding operator

We next give the closed-form solution of (25). It should be noted that the problem (25) is a weighted version with a nonconvex relaxation function $\rho(\cdot)$. In this paper, we employ the popular L_p -function with $p = 1/2$ and $p = 2/3$ as the relaxation surrogates. The reason is that the L_p -function is more flexible, moreover, two special cases of $p = 1/2$ and $p = 2/3$ have been demonstrated their high efficiency and can earn their closed-form solutions [36].

(1) L_p -norm with $p = 1/2$, then the problem (25) is reduced to

$$\sigma_i^*(\mathbf{X}_{G_k}) = \arg \min_{\delta_i > 0} \frac{1}{2} (\sigma_i(\mathbf{X}_{G_k}) - \delta_i(\mathbf{Y}_{G_k}^t))^2 + \xi_i (\sigma_i(\mathbf{X}_{G_k}))^{1/2} \quad (26)$$

then the closed-form of (25) can be defined by [37]

$$\sigma_i^*(\mathbf{X}_{G_k}) = \begin{cases} \frac{2}{3} \sigma_i(\mathbf{X}_{G_k}) \left(1 + \cos\left(\frac{2\pi}{3} - \frac{2}{3} \varphi(\sigma_i(\mathbf{X}_{G_k}))\right)\right), & |\sigma_i(\mathbf{X}_{G_k})| > T \\ 0, & \text{otherwise} \end{cases} \quad (27)$$

where $\varphi(\sigma_i(\mathbf{X}_{G_k})) = \cos^{-1}\left(\frac{\xi_i}{4} \left(\frac{|\sigma_i(\mathbf{X}_{G_k})|}{3}\right)^{-3/2}\right)$, $\xi_i = (\lambda w_{k,i}^t)$, and the threshold value $T =$

$$\frac{3\sqrt[3]{2}}{4} (2\xi_i)^{2/3}.$$

(2) L_p -norm with $p = 2/3$, then the problem (25) is reduced to

$$\sigma_i^*(\mathbf{X}_{G_k}) = \arg \min_{\delta_i > 0} \frac{1}{2} (\sigma_i(\mathbf{X}_{G_k}) - \delta_i(\mathbf{Y}_{G_k}^t))^2 + \xi_i (\sigma_i(\mathbf{X}_{G_k}))^{2/3} \quad (28)$$

then the closed-form of (25) can be defined by [36]

$$\sigma_i^*(\mathbf{X}_{G_k}) = \begin{cases} \left(\left| \theta(\sigma_i(\mathbf{X}_{G_k})) \right| + \sqrt{2 \left| \sigma_i(\mathbf{X}_{G_k}) \right| \left| \theta(\sigma_i(\mathbf{X}_{G_k})) \right| - \left| \theta(\sigma_i(\mathbf{X}_{G_k})) \right|^2 / 2} \right)^3, & |\sigma_i(\mathbf{X}_{G_k})| > T \\ 0, & \text{otherwise} \end{cases} \quad (29)$$

where $\theta(\sigma_i(\mathbf{X}_{G_k})) = \frac{2}{\sqrt{3}} (2\xi_i)^{1/4} \left(\cosh\left(\frac{1}{3} \text{arccosh}\left(\frac{27}{16} (2\xi_i)^{-3/2} (\sigma_i(\mathbf{X}_{G_k}))^2\right)\right) \right)^{1/2}$, $\xi_i =$

$(\lambda w_{k,i}^t)$ and $T = \frac{2\sqrt[4]{3}}{3} (2\xi_i)^{3/4}$ denotes the threshold value.

The whole algorithm for GSC can be summarized in the **Algorithm 1**.

Algorithm 1: Proposed GSC-DNNR algorithm for GSC based denoising optimization model

$$\hat{\mathbf{X}}_{G_k} = \arg \min_{\mathbf{X}_{G_k}} \frac{1}{2} \|\mathbf{Y}_{G_k} - \mathbf{X}_{G_k}\|_F^2 + \lambda \rho_{w_k}(\sigma(\mathbf{X}_{G_k}))$$

Input: The Observation \mathbf{Y} ;

Initialization: $t = 0, \gamma > L_g, \mathbf{X}_{G_k}^0, \mathbf{w}_k^0;$

For $t = 1, 2, \dots$ **do**

While not converge do

1. Updating $\mathbf{X}_{G_k}^{t+1}, \boldsymbol{\alpha}_{G_k}^{t+1}$ by solving (16);

2. Updating the weighting vector \mathbf{w}_k^t by $w_{k,i}^{t+1} \in \partial \rho \left(\rho \left(\sigma_i \left(\mathbf{X}_{G_k}^{t+1} \right) \right) \right);$

End

Output: $\hat{\mathbf{X}}_{G_k}, \boldsymbol{\alpha}_{G_k}^{t+1}.$

III. Integrating GSC based Denoising Model to Image Restoration

Applications via ADMM

In this section, we will integrate the GSC based denoising model to IR problems. Considering the following image degraded model

$$\mathbf{b} = \mathbf{A}\mathbf{x} + \mathbf{n} \quad (30)$$

where $\mathbf{b} \in \mathbb{R}^{\sqrt{M} \times \sqrt{N}}$ denotes the degraded observation, $\mathbf{A} \in \mathbb{R}^{\sqrt{M} \times \sqrt{N}}$ denotes the degradation matrix, $\mathbf{x} \in \mathbb{R}^{\sqrt{N} \times \sqrt{N}}$ and \mathbf{n} are the desired image and the additive noise. Different \mathbf{A} will cause different IR task, when \mathbf{A} is a compressed sampling operator, the IR problem becomes compressive sensing [38], and an identity matrix of \mathbf{A} with entries are either 1 or 0 will often cause image inpainting problem [7]. Suppose the original image $\mathbf{X} \in \mathbb{R}^N$ (also $\mathbf{X} \in \mathbb{R}^{\sqrt{N} \times \sqrt{N}}$) can be represented by the sparse coefficient vector in the domain Ψ , denotes as $\boldsymbol{\alpha} = \Psi\mathbf{X}$, that is $\mathbf{X} = \mathbf{D}\boldsymbol{\alpha}$, where \mathbf{D} denotes the corresponding dictionary, which can be known or learned from the images, and the IR problem can be described as the following generalized optimization model

$$\hat{\boldsymbol{\alpha}} = \arg \min_{\boldsymbol{\alpha}} \mathcal{F}(\mathbf{b}; \boldsymbol{\alpha}) + \lambda \mathfrak{R}(\boldsymbol{\alpha}) \quad (31)$$

where $\mathcal{F}(\mathbf{b}; \boldsymbol{\alpha})$ is the fidelity term and $\mathfrak{R}(\boldsymbol{\alpha})$ denotes regularization term, which measures the sparsity degree of the image and can provide prior knowledge for minimization, such as $\|\boldsymbol{\alpha}\|_p$, the parameter λ denotes the regularization parameter. Then our desired image can be reconstructed by $\hat{\mathbf{X}} = \mathbf{D}\hat{\boldsymbol{\alpha}}$.

3.1 ADMM framework for image restoration via nonconvex weighted group sparse coding

According to the alternative direction method of multipliers (ADMM) framework, we introduce an auxiliary variable \mathbf{z} to the problem (31),

$$\hat{\boldsymbol{\alpha}} = \arg \min_{\boldsymbol{\alpha}, \mathbf{z}} \mathcal{F}(\mathbf{b}; \mathbf{z}) + \lambda \mathfrak{R}(\boldsymbol{\alpha}), \text{ s. t. } \mathbf{z} = \mathbf{D}\boldsymbol{\alpha} \quad (32)$$

Without confusion, we have the following iterative steps:

$$\begin{cases} \mathbf{z}^{(t+1)} = \arg \min_{\mathbf{z}} \mathcal{F}(\mathbf{b}; \mathbf{z}) + \frac{\mu}{2} \|\mathbf{z} - \mathbf{D}\boldsymbol{\alpha}^{(t)} - \mathbf{u}^{(t)}\|_2^2 \\ \boldsymbol{\alpha}^{(t+1)} = \arg \min_{\boldsymbol{\alpha}} \frac{\mu}{2} \|\mathbf{z}^{(t+1)} - \mathbf{D}\boldsymbol{\alpha} - \mathbf{u}^{(t)}\|_2^2 + \lambda \mathfrak{R}(\boldsymbol{\alpha}) \\ \mathbf{u}^{(t+1)} = \mathbf{u}^{(t)} - (\mathbf{z}^{(t+1)} - \mathbf{D}\boldsymbol{\alpha}^{(t+1)}) \end{cases} \quad (33)$$

Then our optimization problem can be split into two subproblems of \mathbf{z} and $\boldsymbol{\alpha}$.

3.1.1 z-subproblem

The \mathbf{z} -subproblem is also a simplified reconstruction step which depends on the forward

model, this paper utilizes the very popular quadratic function to fit the data, e.g., $\mathcal{F}(\mathbf{b}; \mathbf{z}) = \frac{1}{2} \|\mathbf{b} - \mathbf{A}\mathbf{z}\|_2^2$, leading to a quadratic problem, which has a closed-form solution expressed as

$$\mathbf{z} = (\mathbf{A}^T \mathbf{A} + \mu \mathbf{I})^{-1} (\mathbf{A}^T \mathbf{b} + \mu (\mathbf{D}\boldsymbol{\alpha} + \mathbf{u})) \quad (34)$$

where \mathbf{I} denotes the identity matrix. It is efficient to achieve the solution by (34) for image inpainting problem without computing the matrix inverse because of the specific structure in observation matrix \mathbf{A} . However, it will be too time-consuming for CS reconstruction problem. To avoid the computing of matrix inverse, here, a gradient descent method is adopted to solve the \mathbf{z} -subproblem for CS reconstruction by

$$\tilde{\mathbf{z}} = \mathbf{z} - \eta \mathbf{d} \quad (35)$$

where the parameter η denotes the optimal step size, and \mathbf{d} denotes the gradient direction of $\frac{1}{2} \|\mathbf{b} - \mathbf{A}\mathbf{z}\|_2^2 + \frac{\mu}{2} \|\mathbf{z} - \mathbf{D}\boldsymbol{\alpha} - \mathbf{u}\|_2^2$, and we have

$$\mathbf{d} = \mathbf{A}^T \mathbf{A}\mathbf{z} - \mathbf{A}^T \mathbf{b} + \mu (\mathbf{z} - \mathbf{D}\boldsymbol{\alpha} - \mathbf{u}). \quad (36)$$

3.1.2 Denoising operator

After achieving the \mathbf{z} , the $\boldsymbol{\alpha}$ subproblem can be expressed as

$$\boldsymbol{\alpha}^{(t+1)} = \arg \min_{\boldsymbol{\alpha}} \frac{\mu}{2} \|\mathbf{R}^{(t+1)} - \mathbf{D}\boldsymbol{\alpha}\|_2^2 + \lambda \mathfrak{R}(\boldsymbol{\alpha}) \quad (37)$$

where $\mathbf{R}^{(t+1)} = \mathbf{z}^{(t+1)} - \mathbf{u}^{(t)}$ can be regarded as the degraded observation of $\mathbf{z}^{(t+1)}$. It should be noted that the optimization problem (38) is a typical denoising model. To improve the performance for IR problem, we can generate the corresponding group matrix by grouping the similar patches, e.g., \mathbf{R}_{G_k} , \mathbf{D}_{G_k} and $\boldsymbol{\alpha}_{G_k}$. As a result, we have the following equivalent equation with the probability (near to 1) according to following **Theorem 3.1**, e.g.,

$$\|\mathbf{R} - \mathbf{X}\|_2^2 = \frac{N}{K} \sum_{k=1}^n \|\mathbf{R}_{G_k} - \mathfrak{R}(\mathbf{X}_{G_k})\|_F^2 \quad (38)$$

where $\mathbf{X} = \mathbf{D}\boldsymbol{\alpha}$.

Theorem 3.1 [39] *Assume $\mathbf{R}, \mathbf{X} \in \mathbb{R}^{\sqrt{N} \times \sqrt{N}}$, $\mathbf{R}_{G_k}, \mathbf{X}_{G_k} \in \mathbb{R}^{B_s \times c}$, we define $\mathbf{E} = \mathbf{R} - \mathbf{X}$ as the error matrix, and its each element is $\mathbf{E}(j), j = 1, \dots, \sqrt{N} \times \sqrt{N}$. If each element $\mathbf{E}(j)$ is independent and the corresponding distribution of \mathbf{E} with zero mean and variance δ^2 , Then for any $\varepsilon > 0$, we have the following relationship between $\|\mathbf{R} - \mathbf{X}\|_2^2$ and $\|\mathbf{R}_{G_k} - \mathbf{X}_{G_k}\|_F^2$, that is*

$$\lim_{\substack{N \rightarrow \infty \\ K \rightarrow \infty}} P \left\{ \left| \frac{1}{N} \|\mathbf{R} - \mathbf{X}\|_2^2 - \frac{1}{K} \sum_{k=1}^n \|\mathbf{R}_{G_k} - \mathbf{X}_{G_k}\|_F^2 \right| < \varepsilon \right\} = 1 \quad (39)$$

Then optimization problem (37) can be written as

$$\boldsymbol{\alpha}^{(t+1)} = \arg \min_{\boldsymbol{\alpha}_{G_k}} \frac{1}{2} \sum_{k=1}^m \|\mathbf{R}_{G_k} - \mathbf{D}_{G_k} \boldsymbol{\alpha}_{G_k}\|_2^2 + \tau \sum_{k=1}^m \mathfrak{R}(\boldsymbol{\alpha}_{G_k}) \quad (40)$$

where $\tau = \frac{\lambda K}{\mu N}$ with $K = n \times c \times B_s$. According to the theory described in the section 2.2, and by substituting $\mathbf{X}_{G_k} = \mathbf{D}_{G_k} \boldsymbol{\alpha}_{G_k}$, then the problem (38) can be transformed into the following GSC framework based optimization problem,

$$\mathbf{X}^{(t+1)} = \arg \min_{\mathbf{X}_{G_k}} \frac{1}{2} \sum_{k=1}^m \|\mathbf{X}_{G_k} - \mathbf{R}_{G_k}\|_F^2 + \tau \sum_{k=1}^m \mathfrak{R}(\mathbf{X}_{G_k}) \quad (41)$$

where $\mathbf{X}_{G_k} \in \mathbb{R}^{B_s \times c}$ denotes the group matrix with low-rank property. As mentioned before, the denoising model only depends on the prior term, after combining our proposed generalized rank minimization based GSC model, the optimization (41) can be converted into the low-rank matrix recovery problem, that is

$$\mathbf{X}^{(t+1)} = \arg \min_{\mathbf{X}_{G_k}} \frac{1}{2} \sum_{k=1}^m \|\mathbf{X}_{G_k} - \mathbf{R}_{G_k}\|_F^2 + \tau \sum_{k=1}^m \rho_{\mathbf{w}_k}(\sigma(\mathbf{X}_{G_k})) \quad (42)$$

where $\rho_{\mathbf{w}_k}(\sigma(\mathbf{X}_{G_k})) = \sum_{i=1}^r \rho(\rho(\sigma_i(\mathbf{X}_{G_k})))$ denotes the proposed relaxation function. As a result, the optimization problem (42) can be split into m subproblems, and the k , ($k = 1, 2, \dots, m$)-th subproblem can be shown as

$$\mathbf{X}_{G_k}^{(t+1)} = \arg \min_{\mathbf{X}_{G_k}} \frac{1}{2} \|\mathbf{X}_{G_k} - \mathbf{R}_{G_k}\|_F^2 + \tau \sum_{i=1}^r \rho(\rho(\sigma_i(\mathbf{X}_{G_k}))). \quad (43)$$

With this, the optimization problem (43) can be solved by our proposed algorithm in **Algorithm 1**. It should be noted that problem (43) and (16) are two same minimization problems exactly with different regularization parameters τ , therefore, the α -subproblem in IR can be resolved via our proposed nonconvex weighted GSC model.

Then we can achieve the closed-form solution of (43) by **Algorithm 1**, i.e.,

$$\mathbf{X}_{G_k}^{(t+1)} = \mathbf{U}_{R_{G_k}} \text{Prox}_{\rho}^{\delta}(\delta(\mathbf{R}_{G_k}^t)) \mathbf{V}_{R_{G_k}}^T, \quad i = 1, \dots, \min(B_s, c) \quad (44)$$

where $\mathbf{R}_{G_k} = \mathbf{U}_{R_{G_k}} \mathbf{\Sigma}_{R_{G_k}} \mathbf{V}_{R_{G_k}}^T$ denotes its singular value decomposition (SVD), $\mathbf{\Sigma}_{R_{G_k}} = \text{diag}(\xi_{R_{G_k},1}, \dots, \xi_{R_{G_k},\min(B_s,c)})$ and the operator $(\theta)_+ = \max(\theta, 0)$. It should be noted that the sparse coefficient vector α_{G_k} in problem (10) is the singular value vector of matrix \mathbf{X}_{G_k} in our proposed model (see subsection 2.3), hence we can achieve the $\alpha_{G_k}^{t+1}$ simultaneously from (44).

3.2. Summary and Discussion of the proposed algorithm

We first give a whole summary about the proposed algorithm. When all the groups $\{\mathbf{X}_{G_k}\}, k = 1, 2, \dots, n$ are known, then the latent image \mathbf{X} can be reconstructed by

$$\mathbf{X} = \sum_{k=1}^n \mathcal{R}_k^T(\mathbf{X}_{G_k}) ./ \sum_{k=1}^n \mathcal{R}_k^T(\mathbf{1}_{B_s \times c}) \quad (45)$$

where the $\mathcal{R}_k^T(\cdot)$ denotes the transpose grouping operator, $\mathbf{1}_{B_c}$ denotes a column matrix with the size of $B_c \times c$ and all elements being 1, the operator $./$ denotes an element-wise division of two matrix. The proposed whole algorithm of nonconvex weighted GSC for IR via ADMM can be summarized as the **Algorithm 2**.

According to our proposed **Algorithm 2**, we can easily find that our proposed method earns a very important feature of plug-and-play AMMM [40]. Firstly, the denoising model play a key role, which only depends on the image prior model. Secondly, it is very convenient and flexible to employ some other state-of-the art denoising models in our proposed algorithm. From this perspective, an interesting future work is to exploit advanced plug-and-play algorithm to improve the IR performance.

Algorithm 2: Proposed algorithm for IR problem via ADMM

Input: The Observation \mathbf{Y} , the degradation matrix \mathbf{H} ;

Initialization: $c, \mathcal{B}_c, t = 0, \lambda, \mu, \gamma, \mathbf{u}, \mathbf{z}^{(0)}$,
for
 if \mathbf{A} is a mask operator
 Updating \mathbf{z} using the Eq. (34);
 elseif \mathbf{A} is a blur operator
 Updating \mathbf{z} using the Eq. (34);
 else \mathbf{A} is a random projection operator
 Updating \mathbf{z} using the Eq. (35) and (36);
 end
 Computing $\mathbf{R}^{(t+1)} = \mathbf{z}^{(t+1)} - \mathbf{u}^{(t)}$;
 Constructing the groups $\{\mathbf{R}_{G_k}\}$;
 for each group \mathbf{R}_{G_k}
 Construct adaptive dictionary \mathbf{D}_{G_k} using Eq. (4), (5) and (6);
 Reconstruct $\mathbf{X}_{G_k}^{(t+1)}$ and computing $\alpha_{G_k}^{t+1}$;
 end for
 Updating $\mathbf{D}^{(t+1)}$ by concatenating all \mathbf{D}_{G_k} ;
 Updating $\alpha^{(t+1)}$ by concatenating all α_{G_k} ;
 Computing $\mathbf{u}^{(t+1)}$;
 Computing $\mathbf{X}^{(t+1)}$ by concatenating all the dictionaries $\{\mathbf{X}_{G_k}\}$;
 $t = t + 1$;
end
Output: The reconstructed image \mathbf{X} .

IV. Experimental Results

In this section, we will employ the typical L_p , ($p = 1/2, 2/3$) as relaxation of nuclear norm to evaluate the effectiveness of our proposed method for typical IR tasks compared with several state-of-the-art competing IR algorithms. We also analyze the convergence of our proposed algorithm on various IR problems. To measure the reconstruction performance quantitatively, two popular metrics of PSNR and feature similarity (FSIM) [41] will be calculated. The widely used test images are employed to evaluate our proposed method presented in Fig. 3. All the best results will be highlighted in bold in tables, and all the simulation experiments are conducted in a personal computer with Intel (R) Core (TM) i7-6770HQ @ 2.6GHz CPU with 16 GB memory and a Windows 10 operating system.



Fig. 3. Experimental image set. (a), Typical 256×256 gray natural images: Barbara, Boats, Cameraman, Elain, Foreman, House, Leaves, Monarch, Starfish and Straw. (b), Typical 256×256 color images. Top: Barbara, Butterfly, Castle, Clock, Cowboy, Girl, House, Light; Bottom: Mickey, Peepers, Starfish, Vegetable, Zebra, Bike, Fence, Flower and Parrots. (c), Typical 512×512 gray natural images: Couple, Hill and Man.

4.1 Compressive Sensing

CS based image reconstruction technology aims to capture high-quality images from a small number of under-sampling random measurements, in which, one of the main technical challenges is how to obtain high-quality images while reducing the number of measurements. To evaluate the validation of our proposed method, six representative competing CS reconstruction algorithms are employed for comparisons, including the algorithms of BCS [42], SGSR [43], ALSB [39], JASR [44], GSR-Lp [45], GSR-NCR [46]. We empirically set the similar patch parameter $c = 60$, the patch size of $\sqrt{B_s} \times \sqrt{B_s}$ is selected as 6×6 , the block size is 32×32 , and the searching window of $L \times L$ is set to be 20×20 , and $\varepsilon = 0.1$ for all of our CS experiments. The other parameter selections of (μ, λ) are listed in the **Table 2** for different sub-sampling rate and surrogate functions. Table 3 lists all achieved PSNR and FSIM results of four competing algorithms and our proposed method under different sampling rates of 0.1, 0.2, 0.3 and 0.4. We can observe that our proposed rank minimization based GSC method can obtain higher PSNR values and FSIM values than all competing methods. To make a visual comparison, we present the reconstructed results of boats and monarch from 0.1 measurements using our proposed method and other approaches, shown in the Fig. 4 and 5. These visual results demonstrate that our proposed method can reconstruct image with higher quality.

Table 2. The parameter selection for five penalty functions under different sub-rates

Different penalties	0.10	0.20	0.30	0.40
$p = \frac{1}{2}(\mu, \lambda)$	$(8e - 3, 0.10)$	$(3e - 2, 0.30)$	$(5e - 3, 0.01)$	$(2.5e - 2, 0.08)$
$p = \frac{2}{3}(\mu, \lambda)$	$(9e - 3, 0.04)$	$(9e - 3, 0.01)$	$(5e - 3, 0.005)$	$(2.5e - 2, 0.01)$

Table 3. The PSNR (dB)/ FSIM achieved by our proposed algorithm and four competing algorithms

Subrate = 0.100											
Method	Barbara	Boats	C.man	Elaine	Foreman	House	Leaves	Monarch	Starfish	Straw	Averaged
BCS	22.80/0.7891	24.52/0.8029	21.60/0.7605	27.46/0.8811	29.76/0.8911	26.90/0.8455	18.54/0.6852	21.70/0.7828	22.71/0.8049	19.10/0.6559	23.51/0.7899
SGSR	28.70/0.9147	27.71/0.8915	22.60/0.8065	31.32/0.9220	34.88/0.9393	32.77/0.9187	22.22/0.8356	24.27/0.8371	22.91/0.8177	20.24/0.7931	26.76/0.8676

ALSB	27.01/0.8903	27.75/0.8830	23.29/0.8057	30.99/0.9184	33.49/0.9254	32.18/0.9069	21.37/0.7934	24.27/0.8218	23.63/0.8343	20.61/0.7910	26.46/0.8570
JASR	29.58/0.9223	28.59/0.9035	23.54/0.8139	32.01/0.9282	35.61/0.9437	33.49/0.9167	23.62/0.8799	25.83/0.8822	24.39/0.8516	21.02/0.7970	27.77/0.8839
GSR-Lp	28.38/0.9062	28.37/0.8983	24.78/0.8412	31.27/0.9229	35.57/0.9473	33.46/0.9269	25.17/0.9064	26.61/0.9003	24.96/0.8649	21.09/0.7606	27.97/0.8875
GSR-NCR	28.28/0.9217	27.62/0.8977	22.50/0.8006	31.35/0.9318	35.59/0.9449	32.35/0.9128	21.74/0.8367	23.86/0.8289	22.92/0.8227	20.14/0.7904	26.64/0.8688
Proposed ($L_{1/2}$)	29.99/0.9291	29.04/0.9088	24.49/0.8421	32.39/0.9330	36.08/0.9509	34.07/0.9301	25.82/0.9157	27.32/0.9071	25.34/0.8758	21.49/0.8121	28.60/0.9005
Proposed ($L_{2/3}$)	29.77/0.9246	29.12/0.9086	24.59/0.8339	32.20/0.9296	35.95/0.9491	34.02/0.9276	25.93/0.9149	27.34/0.9065	25.58/0.8783	21.57/0.8067	28.61/0.8980

Subrate = 0.200

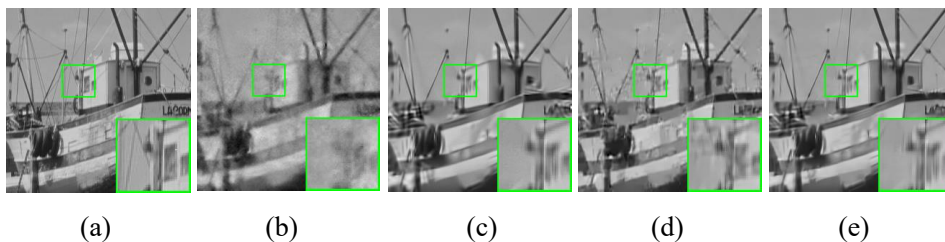
Method	Barbara	Boats	C.man	Elaine	Foreman	House	Leaves	Monarch	Starfish	Straw	Averaged
BCS	24.31/0.8429	27.05/0.8640	24.65/0.8357	31.19/0.9280	32.88/0.9296	30.58/0.9014	21.24/0.7567	25.21/0.8465	25.27/0.8616	20.70/0.7611	26.31/0.8528
SGSR	33.45/0.9615	32.41/0.9465	26.53/0.8850	34.86/0.9551	36.98/0.9598	35.81/0.9502	28.74/0.9373	28.76/0.9132	27.19/0.8993	24.51/0.8854	30.92/0.9293
ALSB	31.77/0.9501	33.04/0.9512	26.53/0.8794	35.11/0.9597	35.33/0.9460	35.93/0.9541	27.14/0.9094	28.39/0.8965	27.20/0.8973	23.88/0.8794	30.43/0.9223
JASR	34.16/0.9651	33.21/0.9521	27.75/0.8961	35.66/0.9603	37.87/0.9636	36.10/0.9425	30.24/0.9516	30.60/0.9409	29.10/0.9295	24.95/0.8913	31.96/0.9393
GSR-Lp	33.74/0.9627	33.34/0.9550	28.47/0.9096	35.72/0.9628	38.65/0.9702	37.02/0.9630	30.33/0.9569	31.04/0.9453	29.01/0.9312	24.73/0.8829	32.21/0.9440
GSR-NCR	33.91/0.9642	33.30/0.9526	26.30/0.8796	35.61/0.9600	37.74/0.9578	36.57/0.9508	28.89/0.9415	29.41/0.9201	27.88/0.9158	24.41/0.8846	31.40/0.9327
Proposed ($L_{1/2}$)	34.62/0.9674	34.03/0.9591	28.38/0.9086	36.15/0.9647	38.79/0.9699	37.18/0.9632	31.44/0.9619	31.79/0.9503	29.96/0.9409	25.12/0.8940	32.75/0.9480
Proposed ($L_{2/3}$)	34.63/0.9676	34.09/0.9596	27.91/0.9051	36.05/0.9650	38.61/0.9699	37.18/0.9656	31.36/0.9621	31.63/0.9482	29.80/0.9400	25.00/0.8933	32.63/0.9476

Subrate = 0.300

Method	Barbara	Boats	C.man	Elaine	Foreman	House	Leaves	Monarch	Starfish	Straw	Averaged
BCS	25.70/0.8780	28.93/0.8995	27.12/0.8798	33.70/0.9512	35.16/0.9504	32.87/0.9298	23.31/0.8062	27.70/0.8839	27.17/0.8954	22.24/0.8288	28.39/0.8903
SGSR	35.91/0.9762	35.22/0.9684	28.81/0.9224	36.87/0.9695	38.47/0.9711	37.37/0.9648	32.98/0.9676	31.99/0.9469	30.79/0.9447	27.33/0.8288	33.57/0.9563
ALSB	34.70/0.9716	36.45/0.9744	28.96/0.9148	37.49/0.9742	36.50/0.9575	38.36/0.9730	31.30/0.9537	31.37/0.9296	30.43/0.9412	26.05/0.9152	33.16/0.9505
JASR	36.59/0.9785	36.08/0.9723	29.93/0.9311	36.83/0.9661	38.54/0.9649	38.04/0.9649	33.70/0.9719	33.63/0.9610	32.33/0.9580	27.88/0.9366	34.36/0.9605
GSR-Lp	35.67/0.9749	35.30/0.9699	30.02/0.9329	37.39/0.9731	40.34/0.9791	38.32/0.9729	33.17/0.9725	33.39/0.9619	31.59/0.9540	26.72/0.9197	34.19/0.9611
GSR-NCR	37.16/0.9815	37.26/0.9783	29.37/0.9305	38.25/0.9774	41.18/0.9829	39.37/0.9795	34.92/0.9799	34.64/0.9666	33.17/0.9654	27.56/0.9348	35.29/0.9677
Proposed ($L_{1/2}$)	37.13/0.9812	37.17/0.9776	29.88/0.9379	38.13/0.9769	41.15/0.9822	39.42/0.9795	35.23/0.9808	34.75/0.9663	33.30/0.9661	27.71/0.9365	35.39/0.9685
Proposed ($L_{2/3}$)	37.18/0.9811	37.11/0.9772	30.06/0.9370	38.20/0.9769	41.11/0.9819	39.38/0.9787	35.17/0.9804	34.81/0.9670	33.26/0.9657	27.89/0.9384	35.42/0.9684

Subrate = 0.400

Method	Barbara	Boats	C.man	Elaine	Foreman	House	Leaves	Monarch	Starfish	Straw	Averaged
BCS	27.19/0.9069	30.60/0.9246	29.13/0.9094	35.70/0.9656	37.04/0.9646	34.67/0.9491	25.23/0.8459	29.75/0.9115	28.97/0.9213	23.77/0.8750	30.21/0.9174
SGSR	37.70/0.9835	37.41/0.9793	30.64/0.9465	38.63/0.9784	39.84/0.9871	38.99/0.9759	35.83/0.9799	34.66/0.9648	33.66/0.9661	29.53/0.9563	35.69/0.9710
ALSB	37.23/0.9830	38.88/0.9838	31.11/0.9441	39.48/0.9830	42.62/0.9871	40.06/0.9820	34.47/0.9730	34.52/0.9581	33.24/0.9642	28.24/0.9468	35.99/0.9705
JASR	37.39/0.9803	37.19/0.9764	31.81/0.9519	38.28/0.9742	41.19/0.9808	38.79/0.9676	36.56/0.9831	36.15/0.9739	34.30/0.9677	30.05/0.9601	36.17/0.9716
GSR-Lp	38.33/0.9854	38.43/0.9832	32.07/0.9563	39.59/0.9828	42.42/0.9866	40.56/0.9834	36.86/0.9860	36.47/0.9767	34.73/0.9735	29.34/0.9539	36.88/0.9768
GSR-NCR	39.22/0.9879	39.63/0.9867	31.59/0.9558	40.08/0.9848	42.95/0.9886	41.11/0.9862	38.51/0.9894	37.58/0.9794	36.21/0.9794	30.05/0.9608	37.69/0.9799
Proposed ($L_{1/2}$)	39.18/0.9875	39.54/0.9861	32.09/0.9590	40.06/0.9844	43.09/0.9881	41.13/0.9855	38.61/0.9895	37.62/0.9794	36.15/0.9791	30.20/0.9617	37.77/0.9800
Proposed ($L_{2/3}$)	39.08/0.9872	39.45/0.9857	32.05/0.9587	39.95/0.9841	43.10/0.9883	41.13/0.9859	38.67/0.9859	37.46/0.9782	36.11/0.9790	30.05/0.9608	37.71/0.9798



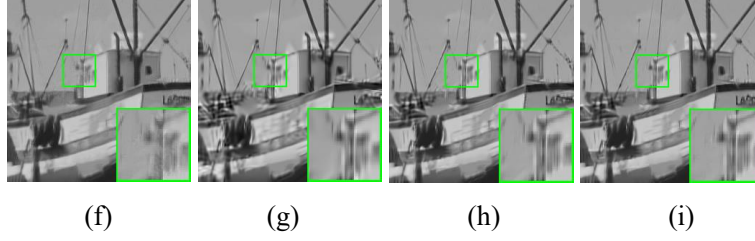


Fig. 4. Original image and eight reconstructed images by BCS, SGSR ALSB, ALSB, JASR and our proposed algorithms for 0.1 measurements of boats. (a) Original Image; (b) BCS, PSNR=24.52 dB, FSIM=0.8029; (c) SGSR, PSNR=27.71 dB, FSIM=0.8915; (d) ALSB, PSNR=27.75 dB, FSIM=0.8830; (e) JASR, PSNR=28.59 dB, FSIM=0.9035; (f) GSR-Lp, PSNR=28.37 dB, FSIM=0.8983; (g) GSR-NCR, PSNR=27.62 dB, FSIM=0.8977; (h) Proposed ($p = 1/2$), PSNR=**29.04** dB, FSIM=**0.9088**; (i) Proposed ($p = 2/3$), PSNR=**29.12** dB, FSIM=**0.9086**;

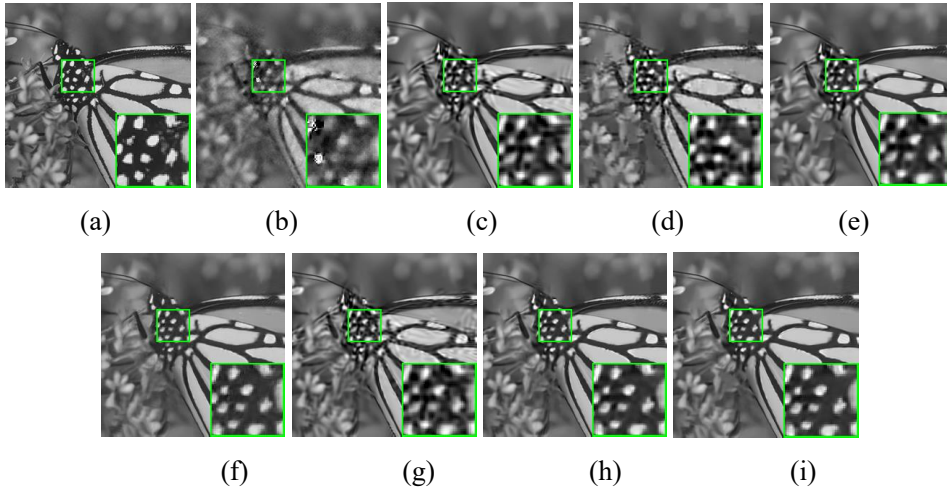


Fig. 5. Visual comparison of the original image and five reconstructed images by BCS, ALSB, ALSB, GSR, JASR and our proposed algorithms for 0.1 measurements of monarch. (a) Original Image; (b) BCS, PSNR=21.70 dB, FSIM=0.7828; (c) SGSR, PSNR=24.27 dB, FSIM=0.8371; (d)ALSB, PSNR=24.27 dB, FSIM=0.8218; (e) JASR, PSNR=25.83 dB, FSIM=0.8822; (f) GSR-Lp, PSNR=26.61 dB, FSIM=0.9003; (g) GSR-NCR, PSNR=23.86 dB, FSIM=0.8289; (h) Proposed ($p = 1/2$), PSNR=**27.32** dB, FSIM=**0.9071**; (i) Proposed ($p = 2/3$), PSNR=**27.34** dB, FSIM=**0.9065**.

4.2 Image Inpainting

For the second applications, we employ our proposed nonconvex framework for image inpainting problem. Image inpainting aims at recovering the missing or damaged pixels in images in a plausible way. In this paper, we focus on two interesting cases of restoration from text removal and partial random samples. Here, the size of each patch is $\sqrt{B_s} \times \sqrt{B_s} = 8 \times 8$ and 10×10 for partial random sample and text removal, respectively. The similar patches number c is set to be 60, and the searching window of $L \times L$ is set to be 20×20 , and $\varepsilon = 0.1$ for all image inpainting experiments, and other parameters selection are listed in the **Table 4**.

Table 4. The parameter selection for different sub-rate and functions

Different penalties	80%	70%	50%	Embed text
$p = \frac{1}{2} (\mu, \lambda)$	(5e - 3, 0.1)	(1e - 3, 0.025)	(1e - 3, 0.01)	(1e - 3, 0.01)
$p = \frac{2}{3} (\mu, \lambda)$	(1.6e - 1, 0.06)	(1e - 1, 0.05)	(3e - 1, 0.0007)	(1e - 2, 0.005)

I. Image restoration from partial random samples

We first handle the IR problem from partial random samples, where the degraded matrix \mathbf{A} is generated by a random matrix. We perform experiments by randomly removing 50%, 70% or 80% of pixels in original images. We employ four state-of-the-art image inpainting algorithms for comparisons, including the algorithms of BPFA [47] (an effective sparse image representations method via Bayesian dictionary learning), IPPO [48] (an IR method based on smooth ordering of patches), Aloha [49] (an recent image inpainting approach based on a low-rank Hankel matrix Approach) and JSM [50] (an IR method using joint statistical modeling scheme). TNNM [33] (a truncated singular value thresholding operator based on the GSC framework), and WNNM [6] (a state-of-the art NNM method). Here, we employ eight color images for experiments. The results achieved by proposed algorithm and other competing state-of-the art algorithms are listed in the Table 5, our proposed approach can outperform other competitive methods significantly.

Table 5. The PSNR (dB)/FSIM values achieved by our algorithm and other four competing algorithms

Missing pixels = 80%											
Method	Butterfly	Bike	Castle	House	Girl	Light	Mickey	Parrots	Vegetable	Zebra	Averaged
BPFA	24.04/0.8533	22.81/0.8469	23.94/0.8639	30.16/0.8987	24.80/0.8766	19.39/0.8091	24.53/0.8696	27.28/0.9285	23.26/0.8672	20.99/0.8190	24.12/0.8633
IPPO	25.13/0.9078	24.04/0.8777	24.50/0.8818	33.65/0.9488	25.31/0.8914	21.51/0.8757	26.33/0.9099	29.16/0.9435	23.07/0.8619	22.71/0.8665	25.54/0.8965
Aloha	24.88/0.8586	23.63/0.8675	23.89/0.8729	33.80/0.9467	25.16/0.8832	21.49/0.8644	25.33/0.8770	29.85/0.9474	23.04/0.8704	22.74/0.8565	25.38/0.8845
JSM	25.58/0.9125	23.56/0.8670	24.57/0.8829	34.28/0.9467	25.18/0.8871	20.20/0.8524	24.57/0.9060	28.46/0.9372	23.29/0.8665	21.86/0.8520	25.16/0.8910
TNNM	26.38/0.9238	24.43/0.8855	24.94/0.8852	35.34/0.9580	25.72/0.8954	22.41/0.8914	26.59/0.9112	29.97/0.9485	23.43/0.8657	22.68/0.8645	26.19/0.9029
WNNM	26.70/0.9291	24.88/0.9029	24.91/0.8959	35.59/0.9592	26.05/0.9094	21.88/0.8936	26.96/0.9212	30.09/0.9517	23.68/0.8866	22.85/0.8816	26.36/0.9131
Proposed ($L_{1/2}$)	26.66/0.9289	24.87/0.9023	25.03/0.8990	35.65/0.9596	26.01/0.9107	22.72/0.9086	27.09/0.9234	30.54/0.9509	23.65/0.8884	23.24/0.8902	26.55/0.9162
Proposed ($L_{2/3}$)	26.39/0.9217	24.45/0.8941	24.66/0.8899	35.15/0.9429	25.72/0.9015	22.07/0.9036	26.85/0.9162	29.97/0.9424	23.46/0.8813	22.63/0.8817	26.14/0.9075
Missing pixels = 70%											
Method	Butterfly	Bike	Castle	House	Girl	Light	Mickey	Parrots	Vegetable	Zebra	Averaged
BPFA	26.52/0.8985	24.85/0.8917	25.68/0.9059	33.96/0.9447	26.61/0.9168	21.36/0.8724	26.17/0.9024	29.91/0.9508	24.66/0.9046	22.73/0.8706	26.25/0.9058
IPPO	27.68/0.9400	26.03/0.9204	26.11/0.9162	36.64/0.9695	27.43/0.9316	23.47/0.9173	28.59/0.9406	32.20/0.9629	24.80/0.9070	24.76/0.9148	27.77/0.9320
Aloha	27.33/0.8998	25.60/0.9130	25.84/0.9103	36.76/0.9691	27.12/0.9215	23.19/0.9066	27.10/0.9104	32.19/0.9641	24.52/0.9099	24.54/0.9003	27.42/0.9205
JSM	27.95/0.9434	25.68/0.9162	26.63/0.9227	36.82/0.9672	27.21/0.9277	23.17/0.9189	28.22/0.9357	31.53/0.9600	24.81/0.9083	23.97/0.9035	27.60/0.9304
TNNM	28.58/0.9452	25.90/0.9125	26.55/0.9122	36.90/0.9652	27.35/0.9217	23.93/0.9198	28.31/0.9315	32.17/0.9576	24.63/0.8951	24.70/0.9032	27.90/0.9264
WNNM	28.78/0.9506	26.39/0.9245	26.74/0.9194	36.90/0.9686	27.50/0.9297	24.20/0.9283	28.70/0.9389	33.05/0.9633	24.96/0.9078	24.93/0.9117	28.22/0.9343
Proposed ($L_{1/2}$)	29.19/0.9530	27.03/0.9362	26.99/0.9269	37.28/0.9712	27.98/0.9384	24.45/0.9342	29.19/0.9448	33.71/0.9676	25.28/0.9181	25.30/0.9222	28.64/0.9413
Proposed ($L_{2/3}$)	29.10/0.9493	26.80/0.9326	26.74/0.9253	37.15/0.9632	28.02/0.9374	24.11/0.9335	29.12/0.9428	33.37/0.9612	25.18/0.9183	24.91/0.9227	28.45/0.9386
Missing pixels = 50%											
Method	Butterfly	Bike	Castle	House	Girl	Light	Mickey	Parrots	Vegetable	Zebra	Averaged
BPFA	30.98/0.9595	29.01/0.9512	28.83/0.9486	39.12/0.9809	30.58/0.9598	25.36/0.9429	29.43/0.9501	33.97/0.9749	27.51/0.9468	26.35/0.9325	30.11/0.9547
IPPO	31.69/0.9724	29.90/0.9639	29.57/0.9576	40.03/0.9853	31.05/0.9672	26.76/0.9591	32.74/0.9719	36.19/0.9820	27.99/0.9536	28.42/0.9528	31.43/0.9666

Aloha	30.78/0.9414	29.78/0.9594	28.71/0.9485	40.56/0.9864	30.60/0.9608	25.83/0.9463	30.33/0.9515	36.14/0.9816	27.06/0.9475	27.70/0.9468	30.75/0.9570
JSM	31.47/0.9719	29.25/0.9618	29.48/0.9588	40.44/0.9853	30.59/0.9662	26.48/0.9594	30.69/0.9685	35.40/0.9805	27.72/0.9536	27.70/0.9545	30.92/0.9661
TNNM	32.09/0.9740	29.76/0.9640	29.63/0.9569	40.76/0.9861	30.89/0.9664	26.79/0.9601	32.23/0.9687	36.17/0.9811	27.64/0.9502	28.21/0.9569	31.42/0.9664
WNNM	33.17/0.9786	31.34/0.9751	29.74/0.9620	41.88/0.9893	32.09/0.9752	26.43/0.9620	33.35/0.9757	37.18/0.9852	28.40/0.9605	28.21/0.9631	32.18/0.9727
Proposed ($L_{1/2}$)	33.23/0.9788	31.41/0.9750	30.29/0.9637	41.80/0.9891	32.14/0.9750	27.53/0.9670	33.91/0.9769	37.87/0.9851	28.51/0.9608	29.32/0.9671	32.60/0.9739
Proposed ($L_{2/3}$)	33.00/0.9778	30.97/0.9729	30.25/0.9629	41.12/0.9873	31.93/0.9732	27.43/0.9661	33.59/0.9749	37.52/0.9837	28.29/0.9594	29.17/0.9652	32.33/0.9723

To further demonstrate the visual effect of our proposed nonconvex framework, Fig. 6 (c) to (j) present nine recovered images from 20% random samples of ‘zebra’ by our proposed method and other state-of-the-art competing methods, and (a) (b) is the original image and the damaged image for comparisons. It can be observed obviously that our proposed method can recover the corrupted image with higher quality and can recover more image details effectively.

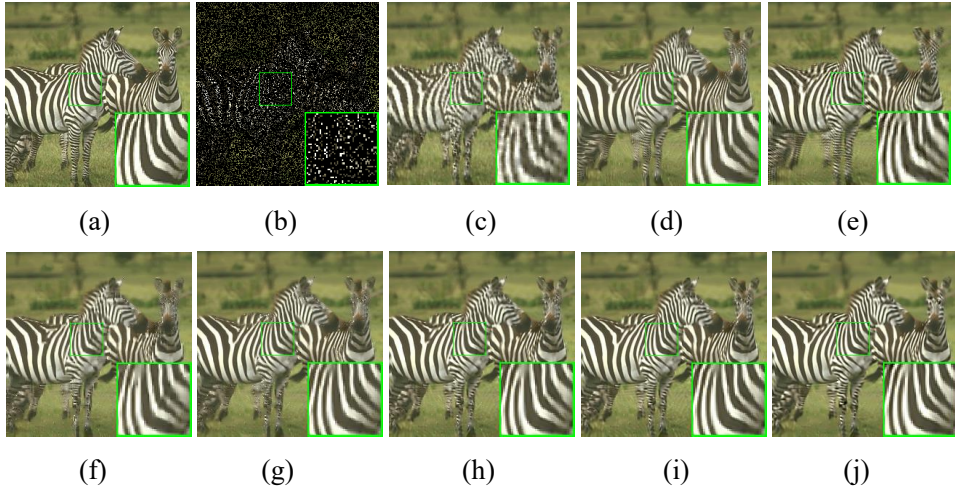


Fig. 6. Visual comparison of the original image, the damaged image, and nine reconstructed images by BPFA, IPPO, Aloha, JSM and our proposed algorithms for 80% missing of zebra. (a) Original Image; (b) The damaged image; (c) BPFA, PSNR=20.99 dB, FSIM=0.8190; (d) IPPO, PSNR=22.71 dB, FSIM=0.8665; (e) Aloha, PSNR=22.74 dB, FSIM=0.8565; (f) JSM, PSNR=21.86 dB, FSIM=0.8520; (g) TNNM, PSNR=22.68 dB, FSIM=0.8645; (h) WNNM, PSNR=22.85 dB, FSIM=0.8816; (i) Proposed ($p = 1/2$), PSNR=**23.24** dB, FSIM=**0.8902**; (j) Proposed ($p = 2/3$), PSNR=22.63 dB, FSIM=**0.8817**.

II. Image inpainting for Text Removal

In this subsection, we will deal with another typical image inpainting problem for text removal, where the degraded matrix \mathbf{A} is generated by a text mask. The goal of text removal is to reconstruct the original image from the degraded observations by removing the text. **Table 6** displays our results achieved by our proposed algorithm and other four state-of-the-art algorithms, our proposed approach can outperform other competitive methods significantly. To make a visual comparison, Fig. 7 (c) to (h) present the case of text removal from a corrupted ‘Mickey’ image, (a) and (b) denote the original image and the corrupted image for comparison. From the results we can find obviously that our proposed method can reconstruct image with more details and can remove more artifacts effectively.

Table 6. The PSNR (dB) values achieved by our proposed algorithm and four competing algorithms

Text Removal											
Method	<i>Barbara</i>	<i>Butterfly</i>	<i>Castle</i>	<i>Clock</i>	<i>Cowboy</i>	<i>Girl</i>	<i>House</i>	<i>Mickey</i>	<i>Peppers</i>	<i>Starfish</i>	Averaged
BPFA	34.13/0.9781	30.81/0.9580	30.25/0.9571	33.10/0.9676	30.43/0.9669	30.46/0.9618	37.65/0.9709	30.92/0.9607	36.04/0.9775	32.65/0.9695	32.64/0.9668
IPPO	37.65/0.9839	33.90/0.9760	31.91/0.9903	36.76/0.9861	32.62/0.9805	32.63/0.9794	41.20/0.9903	34.04/0.9838	39.51/0.9916	35.35/0.9859	35.56/0.9848
Aloha	39.16/0.9906	31.58/0.9569	30.34/0.9672	34.86/0.9770	30.94/0.9741	30.84/0.9693	41.37/0.9889	30.48/0.9641	37.40/0.9866	32.06/0.9719	33.90/0.9747
JSM	37.75/0.9888	33.05/0.9830	32.26/0.9763	35.86/0.9838	32.41/0.9801	32.14/0.9769	41.28/0.9891	32.93/0.9810	39.31/0.9911	35.18/0.9558	35.22/0.9806
TNNM	38.70/0.9908	33.39/0.9818	31.91/0.9746	36.55/0.9851	32.41/0.9788	32.32/0.9767	41.53/0.9903	33.03/0.9804	39.38/0.9911	34.70/0.9839	35.39/0.9834
WNNM	39.54/0.9919	34.12/0.9838	32.60/0.9778	37.36/0.9874	32.93/0.9809	32.81/0.9791	41.88/0.9907	33.83/0.9829	39.93/0.9921	35.44/0.9862	36.04/0.9853
Proposed ($L_{1/2}$)	40.53/0.9934	34.54/0.9849	32.90/0.9797	38.10/0.9895	33.25/0.9827	33.22/0.9811	42.65/0.9923	34.55/0.9853	40.51/0.9932	36.01/0.9880	36.63/0.9870
Proposed ($L_{2/3}$)	40.93/0.9938	34.67/0.9848	32.78/0.9804	38.29/0.9898	33.02/0.9833	33.10/0.9814	42.91/0.9925	34.56/0.9856	40.29/0.9931	36.20/0.9884	36.68/0.9873

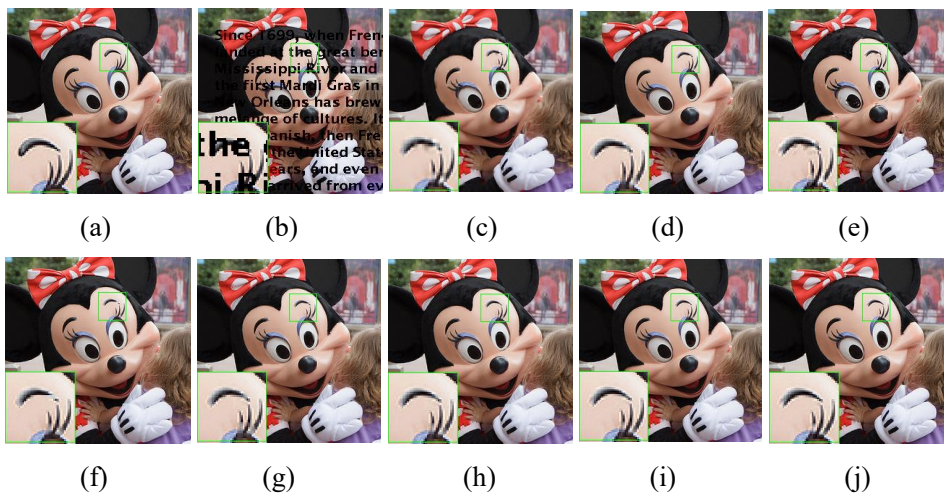


Fig. 7. Visual comparison of the original image, the corrupted image and nine reconstructed images by BPFA, IPPO, Aloha, JSM and our proposed algorithms for text remove of Mickey. (a) Original Image; (b) The corrupted image; (c) BPFA, PSNR=30.92 dB, FSIM=0.9607; (d) IPPO, PSNR=34.04 dB, FSIM=0.9838; (e) Aloha, PSNR=30.48 dB, FSIM=0.9641; (f) JSM, PSNR=32.93 dB, FSIM=0.9810; (g) TNNM, PSNR=33.03 dB, FSIM=0.9804; (h) WNNM, PSNR=33.83 dB, FSIM=0.9829; (i) Proposed ($p = 1/2$), PSNR=34.55 dB, FSIM=0.9853; (j) Proposed ($p = 2/3$), PSNR=34.56 dB, FSIM=0.9856.

4.3 Image deblurring

In this application, we focus on the case of image deblurring, where the blurred image is generated by the blur kernel and Gaussian noise with the standard deviation is σ . In this paper, three typical blur kernels are adopted in our experiments, the 9×9 Uniform blur kernel, the Gaussian blur kernel, and the Motion blur kernel. We compare our proposed nonconvex method to four recently approaches, i.e., MSEPLL [51], GSR-TNNM [33], JSM [50] and WNNM [6]. It should be noted that the method of GSR-TNNM is a recently proposed IR method, and the MSEPLL and JSM are two state-of-the art methods that can often achieve good results for image deblurring problem. The parameter selections for different typical blur kernels and functions are listed in the Table 7. The achieved PSNR and FSIM results on all test images are listed in the Table 8, and Fig. 8, 9 and 10 are presented the recovered under three blur kernels, we can find that our proposed method can produce the best results when the images are corrupted by the uniform blur kernel and the motion

blur kernel. For the case of gaussian blur kernel, though our proposed method cannot achieve the best results in some cases, we still can achieve the higher average vales of PSNRs and FSIMs, and from Fig. 8, 9 and 10 we can see that our method can achieve much sharper image edges and cleaner textures than other methods.

Table 7. The parameter selection for different typical blur kernels and functions

Different penalties	Uniform blur kernel	Gaussian blur kernel	Motion blur kernel
$p = \frac{1}{2} (\mu, \lambda)$	(1e - 2,0.6)	(8e - 3,0.13)	(1e - 2,0.25)
$p = \frac{2}{3} (\mu, \lambda)$	(8e - 2,0.006)	(1.5e - 2,0.003)	(1e - 2,0.005)

Table 8. PSNR/FSIM comparisons for image deblurring

9 × 9 Uniform blur kernel, $\sigma = \sqrt{2}$									
Method	Barbara	Bike	Fence	Flower	Parrots	Pepper	Starfish	Zebra	Averaged
Deblurred	21.74/0.6720	19.56/0.6443	19.57/0.5949	23.53/0.6960	23.85/0.8265	24.03/0.7869	22.55/0.7439	17.82/0.5919	21.58/0.6946
MSEPLL	25.24/0.8791	24.15/0.8570	27.18/0.8990	28.09/0.8847	29.89/0.9246	31.23/0.9309	27.83/0.9045	23.05/0.8593	27.08/0.8924
JSM	25.68/0.8615	23.89/0.8368	27.25/0.9038	26.88/0.8420	27.87/0.8265	28.26/0.8458	26.63/0.8554	23.30/0.8292	26.22/0.8501
GSR-TNNM	26.68/0.8857	24.30/0.8375	28.38/0.9124	28.10/0.8697	29.59/0.9049	30.43/0.9003	27.71/0.8752	23.51/0.8265	27.34/0.8765
WNNM	27.59/0.9033	25.32/0.8637	29.56/0.9302	28.88/0.8856	30.51/0.9088	31.21/0.9121	28.70/0.8989	24.71/0.8678	28.31/0.8963
Proposed ($L_{1/2}$)	27.64/0.9053	25.34/0.8645	29.67/0.9309	28.96/0.8880	30.65/0.9154	31.38/0.9168	28.78/0.9042	23.69/0.8484	28.26/0.8967
Proposed ($L_{2/3}$)	27.40/0.9091	25.07/0.8609	29.76/0.9285	29.21/0.8932	30.87/0.9359	32.14/0.9332	28.75/0.9027	24.30/0.8651	28.44/0.9036
Gaussian blur kernel: fspecial ("gaussian", 25, 1.6) $\sigma = \sqrt{2}$									
Method	Barbara	Bike	Fence	Flower	Parrots	Pepper	Starfish	Zebra	Averaged
Deblurred	22.79/0.7568	22.19/0.7708	22.14/0.6830	26.57/0.8285	26.91/0.8937	27.79/0.8876	25.79/0.8506	20.20/0.7113	24.30/0.7978
MSEPLL	23.83/0.8610	26.00/0.9021	25.97/0.8936	29.98/0.9200	31.49/0.9460	33.28/0.9530	29.98/0.9362	23.64/0.8857	28.02/0.9122
JSM	25.78/0.8738	26.65/0.8890	27.08/0.9028	30.01/0.8956	31.07/0.8928	31.98/0.9097	30.08/0.9122	24.66/0.8726	28.41/0.8936
GSR-TNNM	26.76/0.9012	26.64/0.8854	27.58/0.9128	30.50/0.9108	31.91/0.9338	32.75/0.9279	30.42/0.9191	24.78/0.8711	28.92/0.9078
WNNM	26.55/0.8826	26.50/0.8785	27.31/0.9065	29.71/0.8855	30.96/0.8831	31.40/0.8916	29.74/0.8965	24.73/0.8634	28.36/0.8860
Proposed ($L_{1/2}$)	26.75/0.8952	26.65/0.8844	27.52/0.9111	30.32/0.9045	31.59/0.9148	32.32/0.9158	30.89/0.9301	24.86/0.8809	28.86/0.9046
Proposed ($L_{2/3}$)	26.73/0.9006	26.85/0.8948	27.64/0.9150	30.71/0.9154	32.13/0.9392	33.21/0.9385	30.72/0.9258	24.87/0.8786	29.11/0.9135
Motion blur kernel: fspecial ("motion", 20, 45) $\sigma = \sqrt{2}$									
Method	Barbara	Bike	Fence	Flower	Parrots	Pepper	Starfish	Zebra	Averaged
Deblurred	20.92/0.6678	17.99/0.6303	19.65/0.5641	22.35/0.6966	22.48/0.8201	22.17/0.7656	21.01/0.7520	16.96/0.6009	20.44/0.6872
MSEPLL	25.98/0.8944	25.54/0.8924	25.64/0.8763	28.99/0.9022	31.49/0.9318	30.67/0.9283	27.81/0.9142	24.42/0.8850	27.57/0.9031
JSM	24.95/0.8464	23.19/0.8342	25.40/0.8809	25.69/0.8175	26.48/0.7878	26.38/0.8071	25.14/0.8288	22.60/0.8201	24.98/0.8279
GSR-TNNM	28.45/0.9072	25.76/0.8688	27.55/0.9030	29.63/0.8956	31.56/0.9197	30.96/0.9074	28.28/0.8913	24.56/0.8515	28.34/0.8931
WNNM	29.90/0.9347	27.18/0.9036	28.81/0.9163	30.59/0.9145	33.16/0.9471	33.00/0.9457	30.16/0.9286	25.61/0.8926	29.80/0.9229
Proposed ($L_{1/2}$)	30.14/0.9371	27.40/0.9070	29.05/0.9226	30.71/0.9167	33.13/0.9452	33.03/0.9448	30.34/0.9300	25.88/0.8983	29.96/0.9252
Proposed ($L_{2/3}$)	30.38/0.9397	27.48/0.9070	29.11/0.9228	30.78/0.9171	33.20/0.9463	33.15/0.9463	30.48/0.9309	26.02/0.9001	30.08/0.9263

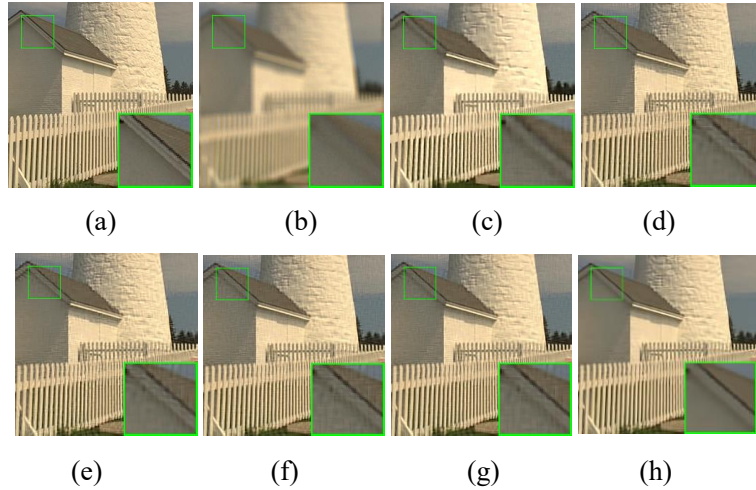


Fig. 8. Restored *Fence* images from corrupted image by 9×9 Uniform blur kernel with $\sigma = \sqrt{2}$ by various methods for visual comparison. (a) Original Image; (b) The deblurred and noisy image, PSNR=19.57 dB, FSIM=0.5949; (c) MSEPLL, PSNR=27.18 dB, FSIM=0.8990; (d) JSM, PSNR=27.25 dB, FSIM=0.9038; (e) GSR-TNNM, 28.38 dB, FSIM=0.9124; (f) WNNM, PSNR=29.56 dB, FSIM=0.9302; (g) Proposed ($p = 1/2$), PSNR=**29.67** dB, FSIM=**0.9309**; (h) Proposed ($p = 2/3$), PSNR=**29.76** dB, FSIM=**0.9285**.

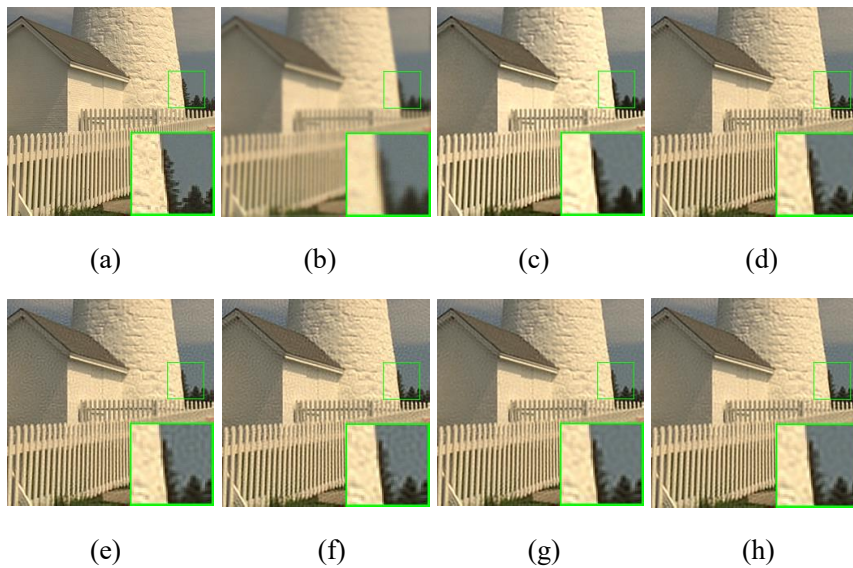


Fig. 9. Restored *Fence* images from corrupted image by Gaussian blur kernel with $\sigma = \sqrt{2}$ by various methods for visual comparison. (a) Original Image; (b) The deblurred and noisy image, PSNR=22.14 dB, FSIM=0.6830; (c) MSEPLL, PSNR=25.97 dB, FSIM=0.8936; (d) JSM, PSNR=27.08 dB, FSIM=0.9028; (e) GSR-TNNM, 27.58 dB, FSIM=0.9128; (f) WNNM, PSNR=27.31 dB, FSIM=0.9065; (g) Proposed $p = 1/2$, PSNR=27.52 dB, FSIM=0.9111; (h) Proposed ($p = 2/3$), PSNR=**27.64** dB, FSIM=**0.9150**.

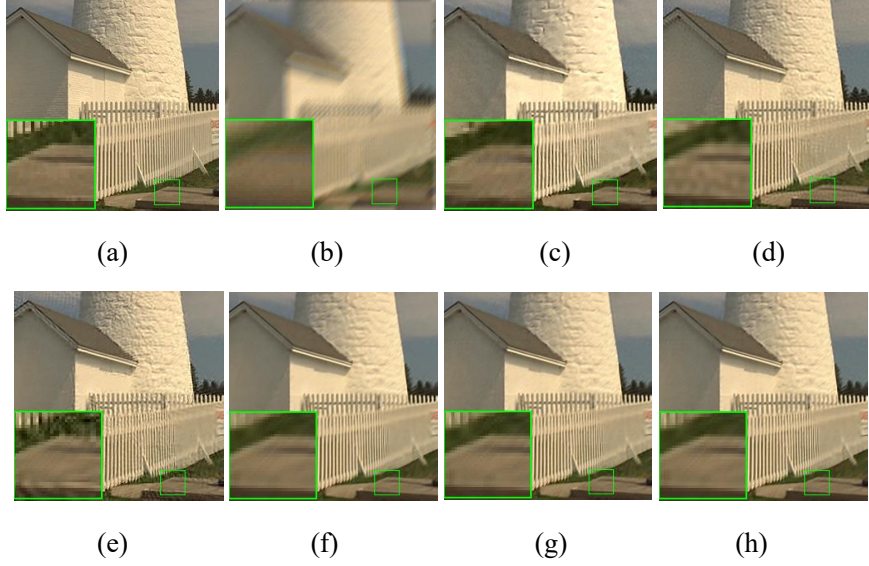


Fig. 10. Visual comparison of the original image, the deblurred and noisy image corrupted by motion blur kernel with $\sigma = \sqrt{2}$. (a) Original Image; (b) The deblurred and noisy image, PSNR=19.65 dB, FSIM=0.5641; (c) MSEPLL, PSNR=25.64 dB, FSIM=0.8763; (d) JSM, PSNR=25.40 dB, FSIM=0.8809; (e) GSR-TNNM, 27.55 dB, FSIM=0.9030; (f) WNNM, 28.81 dB, FSIM=0.9163; (g) Proposed ($p = 1/2$), PSNR=**29.05** dB, FSIM=**0.9226**; (h) Proposed ($p = 2/3$), PSNR=**29.11** dB, FSIM=**0.9228**.

4.4 Salt and Pepper Noise Removal

As a typical impulsive noise, the salt and pepper noise (SPN) usually occurs in the procedure of the image acquisition and transmission. In this application, we will adopt our proposed algorithm to recover the corrupted image by SPN with different strengths, here, five state-of-the-art algorithms of WESNR [52], JSM [50], WCSR [53], TNNM [33] and WNNM [6] are compared with our method. To handle this problem, an adaptive median filter [54] is first applied to the corrupted images, hence we can identify the mask matrix \mathbf{A} , and we can transform the noise removal problem into the IR problem. Table 9 details the parameter selections for different penalties and the noise density. Table 10 presents all the PSNR/FSIM results on six test images, we can find that our proposed method can outperform other three methods significantly. Moreover, some visual results of ‘Cameraman’ for five algorithms are presented in the fig. 11, by comparing with the competing results in (c), (d) and (e), we can obviously find that our method can earn the most visually results, e.g., (f) and (g).

Table 9. The parameter selection for different sub-rate and functions

Different penalties	30% SPN	50% SPN	80% SPN
$p = \frac{1}{2} (\mu, \lambda)$	(1e - 2, 0.15)	(5e - 3, 0.1)	(5e - 3, 0.4)
$p = \frac{2}{3} (\mu, \lambda)$	(1e - 1, 0.05)	(1e - 2, 0.01)	(2e - 2, 0.03)

Table 10. PSNR/FSIM comparison for images corrupted by salt and pepper noise

30% SPN							
Method	<i>Cameraman</i>	<i>Couple512</i>	<i>Hill512</i>	<i>House</i>	<i>Man512</i>	<i>Straw</i>	Averaged
Noisy	10.33/0.4542	10.76/0.6369	10.61/0.5731	10.75/0.4081	10.64/0.5864	10.64/0.6698	10.63/0.5548
WESNR	28.15/0.9303	32.43/0.9800	33.16/0.9827	36.26/0.9548	32.99/0.9816	28.24/0.9442	31.87/0.9623

JSM	30.47/0.9132	32.22/0.9751	31.85/0.9654	35.58/0.9249	31.77/0.9674	27.93/0.9370	31.64/0.9472
WCSR	32.32/0.9704	35.95/0.9940	36.81/0.9939	39.70/0.9861	35.86/0.9935	31.36/0.9769	35.33/0.9858
TNNM	31.86/0.9652	35.08/0.9913	35.76/0.9905	40.73/0.9842	35.10/0.9908	30.88/0.9720	34.90/0.9823
WNNM	33.23/0.9763	36.77/0.9946	37.19/0.9941	42.91/0.9917	36.66/0.9950	33.23/0.9843	36.67/0.9893
Proposed ($L_{1/2}$)	33.24/0.9767	36.85/0.9946	37.30/0.9943	43.11/0.9920	36.79/0.9948	33.37/0.9848	36.78/0.9895
Proposed ($L_{2/3}$)	33.07/0.9749	36.88/0.9946	37.31/0.9940	42.79/0.9903	36.81/0.9944	33.52/0.9853	36.73/0.9889
50% SPN							
Method	<i>Cameraman</i>	<i>Couple512</i>	<i>Hill512</i>	<i>House</i>	<i>Man512</i>	<i>Straw</i>	Averaged
Noisy	8.10/0.3610	8.53/0.5546	8.39/0.4977	8.53/0.4081	8.42/0.5864	8.43/0.5931	8.40/0.5002
WESNR	25.29/0.8901	30.40/0.9665	31.32/0.9675	34.39/0.3188	30.92/0.5075	25.77/0.9039	29.68/0.7591
JSM	28.60/0.8865	30.79/0.9635	30.78/0.9519	34.51/0.9140	30.49/0.9522	25.98/0.9023	30.19/0.9284
WCSR	28.98/0.9383	32.47/0.9842	33.51/0.9852	35.75/0.9681	32.51/0.9837	27.68/0.9479	31.82/0.9679
TNNM	29.32/0.9473	32.85/0.9853	33.74/0.9848	38.44/0.9800	33.05/0.9853	27.97/0.9466	32.56/0.9716
WNNM	30.39/0.9570	33.80/0.9882	34.40/0.9870	39.29/0.9829	33.75/0.9879	29.75/0.9637	33.56/0.9778
Proposed ($L_{1/2}$)	30.65/0.9606	34.27/0.9897	34.92/0.9887	40.08/0.9855	34.24/0.9898	30.35/0.9682	34.09/0.9804
Proposed ($L_{2/3}$)	30.66/0.9601	34.25/0.9896	34.86/0.9883	39.87/0.9841	34.09/0.9893	30.36/0.9682	34.01/0.9799
80% SPN							
Method	<i>Cameraman</i>	<i>Couple512</i>	<i>Hill512</i>	<i>House</i>	<i>Man512</i>	<i>Straw</i>	Averaged
Noisy	6.04/0.3012	6.48/0.4898	6.33/0.4354	6.44/0.2651	6.37/0.4422	6.36/0.5244	6.34/0.4097
WESNR	20.32/0.7907	25.91/0.9058	27.93/0.9210	27.12/0.8595	27.09/0.9194	20.96/0.7439	24.89/0.8567
JSM	24.18/0.7949	26.95/0.9005	27.83/0.8901	30.98/0.8737	27.14/0.8811	20.90/0.6971	26.33/0.8396
WCSR	23.15/0.8340	26.45/0.9302	28.26/0.9435	28.60/0.8906	27.26/0.9366	21.52/0.8250	25.87/0.8933
TNNM	24.40/0.8458	26.79/0.9137	28.10/0.9176	31.61/0.9210	27.57/0.9157	21.09/0.7606	26.59/0.8791
WNNM	25.58/0.8832	28.77/0.9524	29.65/0.9564	34.01/0.9466	29.07/0.9494	24.12/0.8766	28.53/0.9274
Proposed ($L_{1/2}$)	25.62/0.8866	28.85/0.9543	29.77/0.9526	34.10/0.9481	29.13/0.9512	24.32/0.8840	28.63/0.9295
Proposed ($L_{2/3}$)	25.64/0.8876	28.86/0.9551	29.91/0.9525	34.05/0.9451	29.12/0.9510	24.48/0.8914	28.68/0.9305

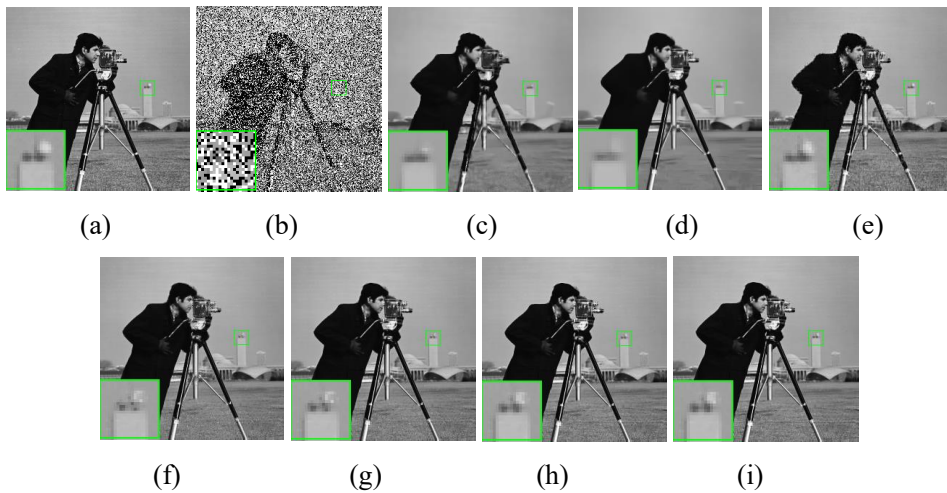


Fig. 11. Visual comparison of the original image, the corrupted image by 50% salt and pepper noise, and five reconstructed images by MSEPLL, GSR-TNNM, JSM and our proposed algorithms. (a) Original Image; (b) The noisy image; (c) WESNR, PSNR=25.29 dB, FSIM=0.8901; (d) JSM, 28.60 dB, FSIM=0.8865; (e) WCSR, PSNR=28.98 dB, FSIM=0.9383; (f) TNNM, PSNR=29.32 dB,

FSIM=0.9473; (g) WNNM, PSNR=30.39 dB, FSIM=0.9570; (h) Proposed ($p = 1/2$), PSNR=30.65 dB, FSIM=0.9606; (i) Proposed ($p = 2/3$), PSNR=30.66 dB, FSIM=0.9601.

4.5 Convergence analysis

Although our proposed method can achieve very effective results, it is intractable to give a theoretical proof of the convergence for our proposed algorithm since the relaxation function of nuclear norm is nonconvex. It is well documented that the behavior of PSNR curves versus the iteration number can reflect the convergence property visually [21][31]. **Fig. 12** (a), (b), (c) and (d) present the PSNRs curves for different IR problems, including the image compressive sensing problem under different sub-sampling rates, image inpainting problem from partial random samples, image inpainting for text removal, and SPN removal. It is obviously that our proposed algorithm contains good convergence property and robustness.

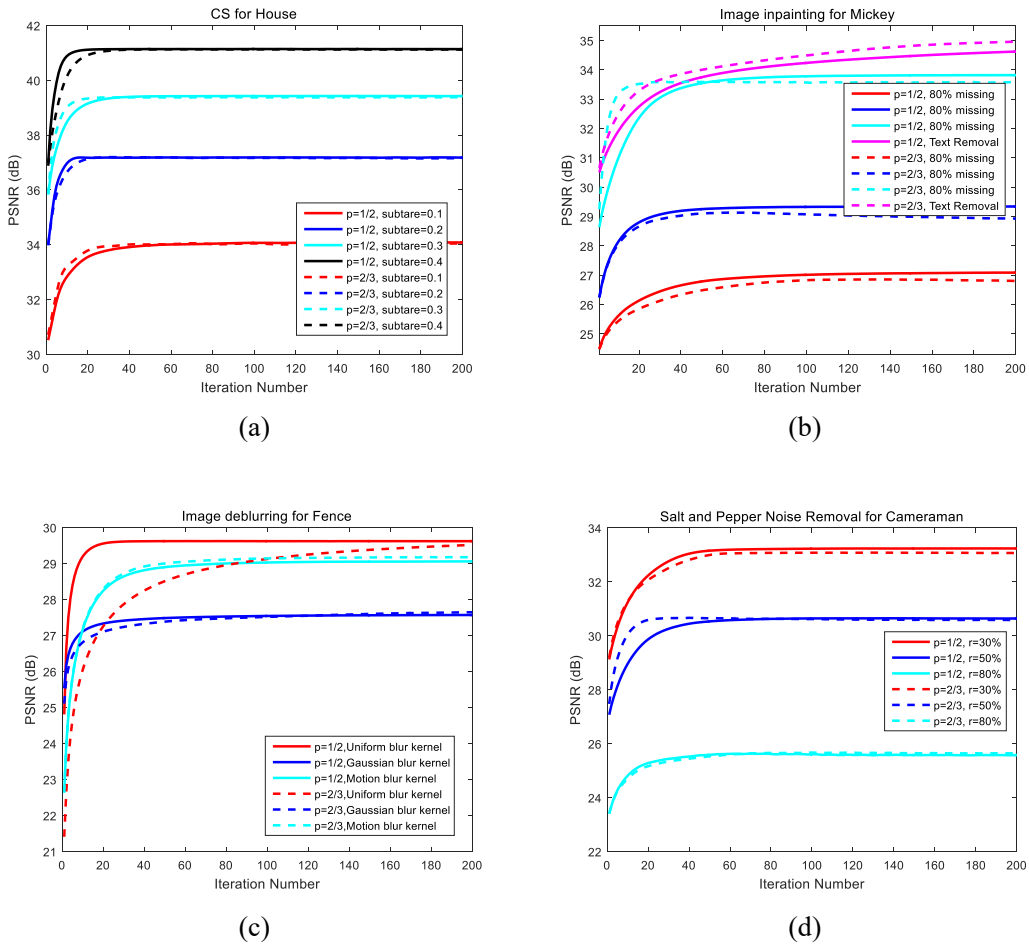


Fig. 12. The verification of the convergence of our proposed method. (a) Image compressive sensing; (b) Image inpainting; (c) Image deblurring; (d) Salt and pepper noise removal.

V. Conclusion

This paper proposed a novel GSC based denoising model via rank minimization for IR applications. We first converted the group sparse coding problem into the low-rank minimization problem via an effective adaptive dictionary learning strategy. To better approximate the rank of the

group matrix, we developed a novel DNNR minimization framework for GSC. To solve this nonconvex optimization problem, an GSC based iteratively-reweighted singular value function thresholding algorithm was proposed. Finally, some typical IR applications have been considered to evaluate the effectiveness and priority of our proposed method via the ADMM strategy.

Acknowledgement

This work was supported by the Project Funded by the National Science and Technology Major Project of the Ministry of Science and Technology of China under Grant TC190A3WZ-2, National Natural Science Foundation of China under Grant 61901228 and 61671253, the Innovation and Entrepreneurship of Jiangsu High-level Talent under Grant CZ0010617002, the Six Top Talents Program of Jiangsu under Grant XYDXX-010, the 1311 Talent Plan of Nanjing University of Posts and Telecommunications.

Reference

- [1] J. Mairal, M. Elad, G. Sapiro, Sparse representation for color image restoration, *IEEE Trans. Image Process.* 17 (2008) 53–69.
- [2] L. Zhang, W. Zuo, Image Restoration: From Sparse and Low-Rank Priors to Deep Priors, *IEEE Signal Process. Mag.* 34 (2017) 172–179.
- [3] K. Zhang, W. Zuo, S. Gu, L. Zhang, Learning Deep CNN Denoiser Prior for Image Restoration, in: 2017 IEEE Conf. Comput. Vis. Pattern Recognit., 2017: pp. 3929–3938. <http://arxiv.org/abs/1704.03264v1>.
- [4] D.L. Donoho, Compressed sensing, *IEEE Trans. Inf. Theory.* 52 (2006) 1289–1306.
- [5] X. Huang, M. Yan, Nonconvex penalties with analytical solutions for one-bit compressive sensing, *Signal Processing.* 144 (2018) 341–351.
- [6] S. Gu, L. Zhang, W. Zuo, X. Feng, Weighted nuclear norm minimization with application to image denoising, in: *Proc. IEEE Comput. Soc. Conf. Comput. Vis. Pattern Recognit.*, 2014: pp. 2862–2869.
- [7] C. Guillemot, O. Le Meur, Image Inpainting: Overview and Recent Advances, *IEEE Signal Process. Mag.* 31 (2014) 127–144.
- [8] J.P. Oliveira, J.M. Bioucas-Dias, M.A.T. Figueiredo, Adaptive total variation image deblurring: A majorization-minimization approach, *Signal Processing.* 89 (2009) 1683–1693.
- [9] S. Wang, Q. Liu, Y. Xia, P. Dong, J. Luo, Q. Huang, D.D. Feng, Dictionary learning based impulse noise removal via L1-L1 minimization, *Signal Processing.* 93 (2013) 2696–2708. <http://dx.doi.org/10.1016/j.sigpro.2013.03.005>.
- [10] F. Wen, P. Liu, Y. Liu, R.C. Qiu, W. Yu, Robust sparse recovery in impulsive noise via Lp-L1 Optimization, *IEEE Trans. Signal Process.* 65 (2017) 105–118.
- [11] F. Wen, R. Ying, P. Liu, T.K. Truong, Nonconvex Regularized Robust PCA Using the Proximal Block Coordinate Descent Algorithm, *IEEE Trans. Signal Process.* 67 (2019) 5402–5416.
- [12] F. Wen, L. Chu, P. Liu, R.C. Qiu, A Survey on Nonconvex Regularization-Based Sparse and Low-Rank Recovery in Signal Processing, Statistics, and Machine Learning, *IEEE Access.* 6 (2018) 69883–69906.
- [13] L. Zhang, Q. Zhang, L. Zhang, D. Tao, X. Huang, B. Du, Ensemble manifold regularized sparse

- low-rank approximation for multiview feature embedding, *Pattern Recognit.* 48 (2015) 3102–3112.
- [14] Y. Li, J. Zhang, S. Fan, J. Yang, J. Xiong, X. Cheng, H. Sari, F. Adachi, G. Gui, Sparse adaptive iteratively-weighted thresholding algorithm (SAITA) for L_p -regularization using the multiple sub-dictionary representation, *Sensors*. 17 (2017) 2920–2936.
- [15] J. Fan, R. Li, Variable Selection via Nonconcave Penalized Likelihood and its Oracle Properties, *J. Am. Stat. Assoc.* 96 (2001) 1348–1360.
- [16] J.H. Friedman, Fast sparse regression and classification, *Int. J. Forecast.* 28 (2012) 722–738. <http://dx.doi.org/10.1016/j.ijforecast.2012.05.001>.
- [17] C.H. Zhang, Nearly unbiased variable selection under minimax concave penalty, 2010. doi:10.1214/09-AOS729.
- [18] M. Jung, X. Bresson, T.F. Chan, L.A. Vese, Nonlocal Mumford-Shah regularizers for color image restoration, *IEEE Trans. Image Process.* 20 (2011) 1583–1598. doi:10.1109/TIP.2010.2092433.
- [19] J. Xu, L. Zhang, W. Zuo, D. Zhang, X. Feng, Patch group based nonlocal self-similarity prior learning for image denoising, in: *Proc. IEEE Int. Conf. Comput. Vis.*, 2015: pp. 244–252.
- [20] W. Dong, L. Zhang, G. Shi, X. Li, Nonlocally centralized sparse representation for image restoration, in: *IEEE Trans. Image Process.*, 2013: pp. 1620–1630.
- [21] J. Zhang, D. Zhao, W. Gao, Group-Based Sparse Representation for Image Restoration, *Image Process. IEEE Trans.* 23 (2014) 3336–3351.
- [22] Y. Liu, X. Yuan, J. Suo, D. Brady, Q. Dai, Rank Minimization for Snapshot Compressive Imaging, *IEEE Trans. Pattern Anal. Mach. Intell.* (2018) 1–18.
- [23] T.-H. Ma, Y. Lou, T.-Z. Huang, X.-L. Zhao, Group-based truncated l_{1-2} model for image inpainting, in: *2017 IEEE Int. Conf. Image Process. (ICIP)*, Beijing, 2017: pp. 2079–2083.
- [24] B. Wen, Y. Li, Y. Bresler, Image Recovery via Transform Learning and Low-Rank Modeling: The Power of Complementary Regularizers, *IEEE Transactions Image Process.* 29 (2020) 5310–5323.
- [25] B. Wen, S. Ravishankar, Y. Bresler, VIDOSAT: High-Dimensional Sparsifying Transform Learning for Online Video Denoising, *IEEE Transactions Image Process.* 28 (2019) 1691–1704.
- [26] Y. Hu, D. Zhang, J. Ye, X. Li, X. He, Fast and accurate matrix completion via truncated nuclear norm regularization, *IEEE Trans. Pattern Anal. Mach. Intell.* 35 (2013) 2117–2130.
- [27] F. Nie, H. Huang, C. Ding, Low-Rank Matrix Recovery via Efficient Schatten p -Norm Minimization, in: *AAAI Conf. Artif. Intell.*, 2012: pp. 655–661.
- [28] C. Lu, J. Tang, S. Yan, Z. Lin, Generalized nonconvex nonsmooth low-rank minimization, in: *Proc. IEEE Comput. Soc. Conf. Comput. Vis. Pattern Recognit.*, 2014: pp. 4130–4137. doi:10.1109/CVPR.2014.526.
- [29] C. Lu, C. Zhu, C. Xu, S. Yan, Z. Lin, Generalized Singular Value Thresholding, in: *Proc. Twenty-Ninth AAAI Conf. Artif. Intell.*, 2015: pp. 1805–1811. <http://arxiv.org/abs/1412.2231>.
- [30] Z. Zha, X. Yuan, B. Wen, J. Zhou, J. Zhang, C. Zhu, A Benchmark for Sparse Coding: When Group Sparsity Meets Rank Minimization, *IEEE Trans. Image Process.* 29 (2020) 5094–5109.
- [31] Z. Zha, X. Yuan, B. Wen, J. Zhou, J. Zhang, C. Zhu, From Rank Estimation to Rank Approximation: Rank Residual Constraint for Image Restoration, *IEEE Trans. Image Process.* 29 (2020) 3254–3269.
- [32] B. Wen, Y. Li, Y. Li, S. Member, A Set-Theoretic Study of the Relationships of Image Models and Priors for Restoration Problems, (2020) 1–15.

- [33] T. Geng, G. Sun, Y. Xu, J. He, Truncated Nuclear Norm Minimization Based Group Sparse Representation, *SIAM J. Imaging Sci.* 11 (2018) 1878–1897.
- [34] C. Lu, J. Tang, S. Yan, Z. Lin, Nonconvex nonsmooth low rank minimization via iteratively reweighted nuclear norm, *IEEE Trans. Image Process.* 25 (2016) 829–839.
- [35] H. Zhang, C. Gong, J. Qian, B. Zhang, C. Xu, J. Yang, Efficient Recovery of Low-Rank Matrix via Double Nonconvex Nonsmooth Rank Minimization, *IEEE Trans. Neural Networks Learn. Syst.* (2019) 1–10.
- [36] W. Cao, J. Sun, Z. Xu, Fast image deconvolution using closed-form thresholding formulas of $L_q(q=1/2,2/3)$ regularization, *J. Vis. Commun. Image Represent.* 24 (2013) 31–41.
- [37] Z. Xu, H. Zhang, Y. Wang, X. Chang, Y. Liang, $L_{1/2}$ Regularization: A Thresholding Representation Theory and a Fast Solver, *IEEE Transactions Neural Netw. Learn. Syst.* 23 (2012) 1013–1027.
- [38] Y. Li, F. Dai, X. Cheng, L. Xu, G. Gui, Multiple-prespecified-dictionary sparse representation for compressive sensing image reconstruction with nonconvex regularization, *J. Franklin Inst.* 356 (2019) 2353–2371.
- [39] J. Zhang, C. Zhao, D. Zhao, W. Gao, Image compressive sensing recovery using adaptively learned sparsifying basis via L_0 minimization, *Signal Processing.* 103 (2014) 114–126.
- [40] S.H. Chan, X. Wang, O.A. Elgendy, Plug-and-Play ADMM for Image Restoration: Fixed-Point Convergence and Applications, *IEEE Transactions Comput. Imaging.* 3 (2017) 84–98.
- [41] L. Zhang, L. Zhang, X. Mou, D. Zhang, FSIM : A Feature Similarity Index for Image Quality Assessment, *IEEE Transactions Image Process.* 20 (2011) 2378–2386.
- [42] Sungkwang Mun, J.E. Fowler, Block compressed sensing of images using directional transforms, in: *Proc. Int. Conf. Image Process.*, 2009: pp. 3021–3024.
- [43] J. Zhang, D. Zhao, F. Jiang, W. Gao, Structural group sparse representation for image Compressive Sensing recovery, in: *Data Compression Conf. Proc.*, IEEE, 2013: pp. 331–340.
- [44] N. Eslahi, A. Aghagolzadeh, Compressive Sensing Image Restoration Using Adaptive Curvelet Thresholding and Nonlocal Sparse Regularization, *IEEE Transactions Image Process.* 25 (2016) 3126–3140.
- [45] C. Zhao, J. Zhang, S. Ma, W. Gao, Non-convex L_p Nuclear Norm based ADMM framewrok for Compressed Sensing, in: *2016 Data Compression Conf.*, 2016: pp. 161–170.
- [46] Z. Zha, X. Zhang, Q. Wang, L. Tang, X. Liu, Group-based sparse representation for image compressive sensing reconstruction with non-convex regularization, *Neurocomputing.* 296 (2018) 55–63.
- [47] M. Zhou, H. Chen, L. Ren, G. Sapiro, L. Carin, Non-parametric Bayesian dictionary learning for sparse image representations, in: *Neural Inf. Process. Syst. (NIPS2009)*, Vancouver, Canada, Dec. 2009, 2009: pp. 1–9.
- [48] I. Ram, M. Elad, I. Cohen, Image processing using smooth ordering of its patches, *IEEE Trans. Image Process.* 22 (2013) 2764–2774.
- [49] K.H. Jin, J.C. Ye, Annihilating Filter-Based Low-Rank Hankel Matrix Approach for Image inpainting, *IEEE Trans. Image Process.* 24 (2015) 3498–3511. doi:10.1109/TIP.2015.2446943.
- [50] J. Zhang, D. Zhao, R. Xiong, S. Ma, W. Gao, Image restoration using joint statistical modeling in a space-Transform domain, *IEEE Trans. Circuits Syst. Video Technol.* 24 (2014) 915–928.
- [51] V. Pappyan, M. Elad, Multi-scale patch-based image restoration, *IEEE Trans. Image Process.* 25 (2016) 249–261.

- [52] Jieliin Jiang, Lei Zhang, Jian Yang, Mixed Noise Removal by Weighted Encoding With Sparse Nonlocal Regularization, *IEEE Trans. Image Process.* 23 (2014) 2651–2662.
- [53] C. Lung, P. Chen, L. Liu, L. Chen, Y.Y. Tang, Weighted Couple Sparse Representation With Classified Regularization for Impulse Noise Removal, *IEEE Transactions Image Process.* 24 (2015) 4014–4026.
- [54] H. Hwang, R.A. Haddad, Adaptive Median Filters: New Algorithms and Results, *IEEE Trans. Image Process.* 4 (1995) 499–502.